INTERNATIONAL ATOMIC ENERGY AGENCY
UNITED NATIONS EDUCATIONAL, SCIENTIFIC AND CULTURAL ORGANIZATION

INTERNATIONAL CENTRE FOR THEORETICAL PHYSICS
34100 TRIESTE (ITALY) - P.O.B. 586 - MIRAMARE - STRADA COSTIERA 11 - TELEPHONE: 2940-1
CABLE: CENTRATOM - TELEX 460392-1

H4.SMR/204 - 37

WINTER COLLEGE ON

ATOMIC AND MOLECULAR PHYSICS

(9 March - 3 April 1987)

LASER SPECTROSCOPIC APPLICATIONS

S. SVANBERG

Lund Institute of Technology
S-221 00 Lund
Sweden

LASER-SPECTROSCOPIC APPLICATIONS

Atomic and Molecular Spectroscopy
Chapter 10

In preparation for
Springer Series in Optical Sciences

Sune Svanberg
Department of Physics
Lund Institute of Technology
1987

10. LASER-SPECTROSCOPIC APPLICATIONS

In the previous chapter we have seen how tunable lasers can be used in a multitude of ways for gaining basic information on atomic and molecular systems. Thus, while the laser has had a very large impact on basic research its utility within the applied spectroscopic field is not smaller. We shall here discuss some applications of considerable interest. Previously, we have mainly chosen atomic spectroscopic examples rather than molecular ones, but in this chapter we shall mainly discuss applied molecular spectroscopy. First we will describe diagnostics of combustion processes and then discuss atmospheric monitoring by laser techniques. Different aspects of laser-induced fluorescence in liquids and solids will be considered with examples from the environmental, industrial and medical field. We will also describe laser-induced chemical processes and isotope separation with lasers. Finally, spectroscopic aspects of lasers in medicine will be discussed.

10.1 Diagnostics of combustion processes

10.1.1 Background

Lately, research in the combustion field has been intensified because of the appreciation of the need for efficient combustion combined with low pollution formation. In order to get a deeper understanding of combustion processes it is necessary to perform the study on a molecular level. Laser-spectroscopic techniques provide unique possibilities of non-intrusive measurements on the extremely aggresive media, that burning or exploding gases constitute. Because of the unique properties of laser beams, both high spatial and temporal resolution can be achieved. Before we describe some measurement techniques we will give an elementary background to combustion processes.

A detailed understanding of combustion must start with simple processes such as hydrogen, methane or acteylene combustion in oxygen or air. Normal liquid hydrocarbons are considerably more complex whereas wood or coal combustion hardly can be attacked on a molecular level. Below we give some "effective" chemical reactions leading to a transformation of fuel and oxidant into carbon dioxide and water. The processes are strongly exothermic, which is of course a common feature for combustion processes.

Flame	Effective Reactions	Temperature(K)	Energy release(J/g)
H_2/O_2	$2H_2+O_2 \rightarrow 2H_2O$	3,100	24,000
CH_4/O_2	$CH_4+2O_2 \rightarrow CO_2+2H_2O$	3,000	10,000
C_2H_2/O_2	$2C_2H_2+5O_2 \rightarrow 4CO_2+2H_2O$	3,300	12,000

Combustion occurs with a large number of intermediate steps and even simple processes such as the ones listed above occur through dozens of coupled elementary reactions. With computer simulations it is possible to describe the interaction between the reactions and concentration profiles can be calculated. In order to accomplish the computer calculations is is necessary to know the rate constants for the individual elementary reactions. Comparisons between theory and experiments are best made for a flat, premixed flame, which in its central part can be considered to have only one-dimensional (vertical) variation, allowing computer calculations to be performed comparatively easy. In the computer description the most important reactions are included. In Fig. 10.1 experimental and theorectically calculated concentration curves are given for the case of low-pressure ethane/oxygen combustion.

Fig. 10.1 here.

As examples of important elementary processes we give the reactions below:

$$CO + OH \rightarrow CO_2 + H$$

$$H + O_2 \rightarrow O + OH$$

Reactive molecular fragments or radicals, such as OH, H and O are very important in combustion. The combustion zone of a stochiometric CH_4/O_2 flame contains about 10 % OH, and 5 % of H and O each. In the latter of the two reactions given above the number of radicals is doubled. A fast increase in radical formation frequently leads to explosive combustion. Because of the high reactivity of radicals they cannot be measured by probe (extraction tube) techniques, since wall reactions immediately eliminate them. Thus laser techniques are particularly valuable for radical monitoring. Pollution formation in flames should also be considered. Nitrogen and sulfur oxides, incompletely burnt hydrocarbons and soot particles form important pollutants. It is of outmost importance to understand which elementary reactions form and elimate pollutants, respectively. The formation of nitric oxide is reasonably well understood. At temperatures above 2000 K the nitrogen of the air is attacted:

$$O + N_2 \rightarrow NO + N$$
$$N + O_2 \rightarrow NO + O$$

The two reactions constitute the so called Zeldovich mechanism. NO is then oxidized to the toxic NO_2 by the oxygen of the air. NO can be elimated from the post flame gases by addition of NH_3. The following reactions occur [10.1]:

$$NH_3 + OH \rightarrow NH_2 + H_2O$$
$$NO + NH_2 \rightarrow N_2 + H_2O$$

For the case of sulphuroxide SO it is immediately further oxidized to SO_2 in the flame. It seems like a reduction of SO_2 can only be obtained by using low sulphur fuels. SO_2 and NO_2 are further oxidized to H_2SO_4 and HNO_3 in the atmosphere with subsequent acid rain formation.

Soot formation is presently much studied. Soot formation is enhanced at high fuel/air mixing ratios (rich flames), when using hydrocarbons with comparatively little H and for bad mixing conditions. Since available fuels will be successively more poor in H, soot formation will become on increasing problem. The chemistry of soot formation is not well understood. Many processes including polymerization of simple hydrocarbons to heaver ones and reactions with polyaromatic hydrocarbons may be important. Basic flame combustion is described in Refs [10.2-3] and emission and absorption spectroscopy of flames are discussed in Ref. [10.4].

Laser techniques have a great potential for studies of microscopic as well as macroscopic combustion in flames and engines. Combustion diagnostics with laser is discussed in several reviews [10.5-8]. We will here give examples of measurements of concentrations and temperature (flame kinetics) using fluorescence, Raman and coherent Raman techniques. In practical combustion systems turbulence is extremely important and we will also briefly mention laser techniques for flow and turbulence measurements.

10.1.2 Laser-induced fluorescence (LIF) andrelated techniques

In laser-induced fluorescence (LIF) experiments a laser is normally tuned to an allowed dipole transition from a lower to an upper state of the species under consideration and fluorescence light, that is released at the subsequent decay is observed. We will start this section by considering the corresponding spontaneous emission process. At the high temperatures in a flame, upper levels become thermally populated and a natural emission giving the flame its colour occurs. In fig. 10.2 part of the emission spectrum from a C_3H_8/air Bunsen burner flame is shown, featuring storng bands due to the radical C_2. This emission was described by Swan already in 1857 in one of the earliest molecular spectroscopy experiments. C_2 is responsible for the blue-green light from the lower parts of hydrocarbon flames. A schematic energy-level diagram for C_2 with the wavelengths of the individual bandheads is shown in Fig. 10.3.

Fig. 10.2 here

Fig. 10.3 here

Hydrocarbon flames also exhibit strong bands due to the CH (~390 and 430 nm) and the OH radicals (~300 nm). In sooty flames the strong yellow light is due to incendescence of soot particles.

LIF yields a much more well-defined emission situation than the one pertaining to the thermal emission. However, for quantitative LIF measurements it is necessary to consider and control the quenching of the fluorescence because of collisional, radiationless transitions. The quenching can be represented by a term Q to be accounted for on equal footing with A (describing spontaneous emission). The observed light intensity will be strongly reduced due to the strong but rather unpredictible degree of quenching. Eq. (9.X), describing saturation now must be written:

$$\frac{N_2}{N_1+N_2} = \frac{\frac{1}{2}}{1+\frac{A+Q}{2B\rho(\nu)}} \qquad (10.1)$$

Since Q is frequently 10^3 times larger than A a very high spectral energy density $\rho(\nu)$ is needed to obtain saturation with a laser beam. However, this can often be achieved and then the maximum fluorescence intensity is obtained despite the quenching, which no longer influences the measurement. Alternatively, the degree of quenching can be measured directly by time-resolved fluorescence spectroscopy. This is possible, since the lifetime τ is shortened from its natural value 1/A to 1/(A+Q). With a prior knowledge of the low-pressure "true" lifetime value the observed value immediately yields the quenching at the particular pressure. Clearly, the quenched lifetimes are normally very short and have to be measured by picosecond laser techniques (See Section XX) [10.9].

An experimental set-up for studying LIF in flames is shown in Fig. 10.4. The output of a Nd:YAG pumped dye laser can be frequency doubled and if needed the doubled output can be mixed with residual 1.06 μm radiation to achieve still shorter wavelenghts. The beam is directed through the flame and the fluorescence can be spectrally analyzed with the spectrometer shown in the upper part of the figure. In the lower part of the figure it is shown how a diode-array detector can be used to obtain a one-dimensional image of the distribution of a radical across a flame

[10.10]. The streak of LIF is imaged onto the detector, which is gated with the laser firing. Fig. 10.5 shows distributions of OH fluorescence at various heights in a CH_4/O_2 flame. A single 10 ns pulse is used for each recording.

Fig. 10.4 here. Fig. 10.5 here.

Using matrix detectors or Vidicon tubes the LIF imaging techniques can be extended to two-dimensional imaging [10.11]. Using single-photon LIF, many flame species including OH, C_2, CN, CH and NO have been studied.

Several important flame species have their single-photon excitation wavelenghts in the VUV region, where the flame gases absorb and tunable lasers are not readily available. It is then possible to use two-photon or even three-photon excitation (See Section 9.1). In Figs. 10.6 and 10.7 an excitation scheme and a 2-photon LIF spectrum for oxygen atoms in a C_2H_2/O_2 welding torch are shown. The collisional transfer from the triplet to the quartet system in O should be especially noted.

Fig 10.6 here. Fig. 10.7 here.

Hydrogen atoms can be detected observing Hα or Hβ emission from the n = 3 or 4 levels following two- or three photon excitation [10.12]. CO molecules are also best detected using two-photon excitation [10.13]. The excitation of flame species to an upper level can also be detected by other means. Thus optogalvanic spectroscopy (Section 9.x) [10.14] and photoacoustic spectroscopy (Section 9.x) [10.15] employing pulsed lasers have been used. The former method is not non-intrusive in nature because of the need for electrodes. The latter technique utilizes the local pressure increase following excitation and for the detection a microphone close to the flame is used. Spatial resolution is limited since the signal is collected along the laser beam. Ordinary absorption measurements clearly constitute the best examples of such line-of-sight measurements. Diode lasers as well as dye lasers have successfully been used in flame absorption measurements [10.16]. With tomographic techniques, similar to those used in medical X-ray imaging [10.17], spatially resolved information can be

obtained from integrated absorption measurements in different directions through the flame [10.18]. Laser beam deflection can also be used to detect optical resonance. In the region of optical excitation the index of refraction of the gas changes and a probing laser beam (frequently a He-Ne laser beam) crossing the excited region will be deflected [10.19].

10.1.3 Raman spectroscopy

Because of its insensitivity to quenching (the lifetime of the virtual state is $\sim 10^{-14}$s), Raman spectroscopy is of considerable interest for quantitative measurements on combustion processes. Further, important flame species such as O_2, N_2 and H_2 that are only Raman-active (See Section 4.X) can be readily studied with this technique. However, because of the inherent weakness of the Raman scattering process (Section 4.X) only non-luminous (non-sooting) flames can be studied.

Extractive Raman measurements on stable flame species can readily be performed. Here gases are transferred from the flame through a thin tube to the scattering cell of a laser Raman gas analyzing system. In Fig. 10.8 Stokes Raman spectra from the lower and upper part of a C_3H_8/air Bunsen-burner flame are shown as obtained using an Ar^+ laser operating on the 488 nm line. The conversion of fuel and O_2 into CO_2 and H_2O, constituting the over-all combustion process, is clearly demonstrated. The H_2O

Fig. 10.8 here

signal does not increase because of a water-vapour condenser in the feeding gas line. Soot particles, that give rise to a broad-band LIF background are also filtered away. The lower trace also displays signals due to CO and H_2, gases that will mostly burn up higher up in the flame. The weak signals in the shoulder of the strong Rayleigh line in the lower trace are due to pure rotational Raman transitions in the H_2 molecule, which because of its small mass has an exceptionally large rotation constant B (Section 3.X). The main hydro-carbon signal at about 570 nm has many components correponding to slightly different C-H stretch vibrational frequencies. Overtone and combination bands are also observed at smaller Raman shifts.

Using pulsed lasers and gated detection electronics, Raman measurements can also be performed for major species in flames, that do not contain too many particles. Temperature measurements can then also be made using the Stokes/anti-Stokes signal asymmetry or the occurrence of slightly displaced Stokes hot-bands as discussed in Section 4.X. Flame Raman spectroscopy is discussed in further detail in Ref. [10.20].

10.1.4 Coherent Anti-Stokes Raman Scattering (CARS)

The CARS process has previously been described (Section 8.6). CARS spectroscopy is of particular interest for combustion diagnostics because of the strong signal available as a new laser beam emerging from the irradiated gas sample. Thus CARS is largely insensitive to the strong background light that characterizes practical combustion systems such as industrial flames and internal combustion engines. We recall, that the spectroscopic information is contained in the third order susceptibility term $\chi^{(3)}$. This term is given by sum a of a complex resonant term, (proportional to the concentration of the studied molecule) and a non-resonant background term. Thus, when the expression $|\chi^{(3)}|^2$ governing the signal strength is formed (Eq. 8.11) interference between the resonant signal and the background occurs resulting in asymmetric signals, very much like in polarization spectroscopy (Section 9.X). For a molecule with vibrational and rotational levels, that are populated depending on the temperature, there are many close-lying resonances and the signal shape has to be calculated with a computer program. In Fig. 10.9 theoretical curves for the N_2 molecule are shown for different temperatures. The occurrence of the first hot-band and the gradual widening of the vibrational peaks due to increasing

rotational level population can clearly be seen for increasing temperatures. Fig. 10.10 shows experimental spectra for a CH_4/air flame and for room temperature air recorded with a set-up of the type shown in Fig. 10.11.

Fig. 10.9 here Fig. 10.10 here

The BOXCARS phase-matching scheme [8.x.x] is illustrated for the pump beams at ω_p and the Stokes beam at ω_s. After frequency doubling the main part of the Nd:YAG laser output is used for pumping the dye laser, that generates the tunable ω_s beam, whereas the rest is used for the pump beam. The anti-Stokes beam at $\omega_{AS} = 2\omega_p - \omega_s$, emerging when $\omega = \omega_p - \omega_s$ matches a rotational-vibrational transition for the molecule, is detected after proper spectral isolation from the strong pump beam. When the dye laser is slowly tuned through the signal region with the laser continuously firing, curves such as the ones shown in Fig. 10.10 are recorded using a boxcar gated integrator. The resolution in the spectrum is given by the (small) laser linewidths and not by the resolution of a spectrometer as in normal spontaneous Raman spectroscopy.

Fig. 10.11 here

Because of the highly non-linear nature of the CARS process (the signal is proportional to the square of the molecular number density and to $I_p^2 I_s$, Eq. (8.11)) signal averaging does not yield a true value for rapidly varying, turbulent media. It is thus desirable to be able to perform the measurement using a single laser pulse. This is possible using an amplified broad-band dye laser (Section 8.X) for the Stokes beam that in conjunction with a narrow-band pump-laser beam will cover all the difference frequencies $\omega_p - \omega_s$ of interest for a specific molecular spectrum. The anti-Stokes signal frequency components are then all generated simultaneously through the action of the third order susceptibility $\chi^{(3)}$. A gated and intensified linear diode array is used for capturing the single pulse spectrum. The technique can be used for measurements in specially adapted internal combustion engines. The laser firing can be strobed on a particular crank-angle and the temperature at various time intervals can then be assessed. An experimental spectrum from N_2 molecules in a firing internal combustion engine is shown in Fig. 10.12. CARS techniques have also been applied to full scale coal furnaces [10.21]. CARS is especially useful for remote thermo-

Fig. 10.12 here

metry but also species concentrations can be determined, especially for major species. CARS techniques are discussed in more detail in Refs. [10.22-24]. For minor species LIF is frequently the most suited technique. Since the LIF signals also depend on the population of the initial level, temperature can also be determined in such experiments if excitations from two metastable levels with different energies are used (Two-line fluorescence method [10.25].

The techniques discussed here in connection with combustion diagnostics can clearly also be used for monitoring of other reactive media. Thus spark and ignition phenomena can be studied [10.26] as well as processes in chemical reactions [10.27-28]. The techniques have also been found to be valuable in the characterization of chemical vapour deposition (CVD) processes for semiconductor fabrication [10.29-30].

10.1.5 Velocity measurements

Laser Doppler Velocimetry (LDV) is an important non-spectroscopic laser technique for intrusion-free measurements of velocities in liquid or gaseous flows, including combustion flows. In this technique two laser beams (frequently from an Ar^+ laser) are crossed at a small angle in the medium to be studied as shown in Fig. 10.13. A standing interference pattern with bright and dark fringes is then formed. If a small particle, that is carried by the flow passes the interference pattern it will produce periodic glimpses of light that can be detected by a photo-multiplier tube. The frequency of the periodic signal (the Doppler burst) can be analyzed by Fourier transformation (See page XXX) and the velocity v can then be determined since the fringe separation d is given by the laser wavelength λ and the beam crossing angle α.

We have v =

(10.2)

Clearly, if the particle is larger than the fringe separation contrast is reduced and thus LDV measurements also provide information on the particle sizes.

Fig. 10.13 here.

With one pair of crossing laser beams only one velocity component in the flow field is determined. Furthermore, it is not possible to determined the sign of that velocity component since either flow direction produces the same Doppler burst. However, by frequency shifting one of the crossing beams with a Bragg cell (acoustooptic modulator), moving interference fringes are produced. Then it is possible to decide from which direction a particle passed the interference field by noting if the burst frequency was shifted upwards or downwards from the frequency from a fixed object. A second velocity component can be measured by using two additonal laser beams propagating in a plane perpendicular to the first laser beam plane and crossing at the same point. In order to be able to distinguish the Doppler burst from this interference pattern, different wavelenghts are used for the laser beams. Thus, it is customary to use the 5145 Å line of an Ar^+ laser for the one velocity component and the 4880 line for the other one. The elastically scattered light is then detected through sharp interference filters in front of individual photomultiplier tubes. The third velocity component (in the direction of the bisectrice of the crossing laser beams) is harder to measure. However, by using three crossing beams in the same plane and extracting the information pair-wise from the central beam and one or the other of the external beams the third velocity component can be projected out, although at lower accuracy. When the scattered intensity is low, e.g. because of small particles, it is still possible to extract velocity information from the time correlation of the recorded individual photons. Special auto-correlation techniques have been developed for an optimum

information extraction [10.31]. Frequently it is necessary to seed the flow with small particles. These particles do not necessary truly follow the gas flow, which constitutes a complication with this technique.

We should conclude this description of LDV techniques with a comment on its common name. In our description of the technique we have not used a Doppler language at all but rather expressed the observed phenomena in terms of a spatial interference pattern. However, alternatively we can consider the Doppler shift in the scattered light frequency caused by the motion of the particle. This shift is detected as a beat frequency against the light scattered from the other crossing beam. The beat frequency exactly corresponds to the frequency produced by a particle crossing the fringe pattern, so the two pictures are as a matter of fact equivalent. LDV techniques are discussed in detail in the monographs [10.32-33].

A further class of velocity measurement techniques use molecular "tagging" using a first pump pulse. The movement of the tagged package of molecules is then monitored with a second laser beam [10.34].

We will also consider a technique for velocity measurements, which is based on Doppler shifting of absorption lines of atoms or molecules in the flow [10.35]. The principle of the technique is illustrated in Fig. 10.14. A narrow band CW laser is

Fig. 10.14 here.

tuned to a frequency ν in the shoulder of a Doppler broadered absorption line, where fluorescence light of half the maximum intensity can be induced. If the gas molecules are displaced by a flow the whole Doppler-broadended profile will shift in frequency. Depending on the direction of this flow the fluorescence light intensity will increase or decrease. In order to measure the presence of a net flow, two alternate laser beams are sent through the medium in opposite direction. The fluorescence intensities are balanced out for a static gas, by adjusting the

relative powers in the two beams. If the gas is moving a modulation will be observed at the frequency of the beam direction shifting. By normalizing the signal it becomes independent of the number density of the molecules.

$$\text{We have } v = \frac{c}{\nu} \frac{I_{left} - I_{right}}{I_{left} + I_{right}} \cdot \frac{g(\nu)}{(dg/d\nu)} \qquad (10.3)$$

where I_{left} and I_{right} are the two detected fluorescence intensities and $g(\nu)$ is the value fo the line shape function at the chosen frequency ν.

A single-mode CW dye laser can be used for measurements of this kind. The experimental set-up is similar to the one used in Doppler-free inter-modulated fluorescence measurements (See page XXX), but now the beams are presented to the atoms/molecules only one at a time. For measurements of this kind sodium atoms or I_2 molecules can be seeded to the flow. Imaging measurements using array detectors as discussed above can be performed. In Refs [10.36-37] imaging measurements of species concentrations, temperatures and flows utilizing LIF are described.

10.2 Laser remote sensing of the atmoshere

Different aspects of remote sensing have been discussed in Sections 6.6 and 7.2. In this section we will describe how laser techniques can be used for monitoring of the atmosphere and its pollutants. General information on the atmosphere and its optical properties is given in Ref. [10.38-40]. Laser beams are particularly useful for monitoring over large distances because of the low divergence of the beam. Typically a divergence of 0.5 mrad is obtained, corresponding to a spot diameter of 0.5 m in 1 km distance. Dry air contains 78.1 % of N_2 and 20.9 % of O_2. The noble gases Ar, Ne and He are present at 9300, 18 and 5 ppm (parts per million) respectively. The CO_2 contents is presently 320 ppm, a value that is increasing annually by 0.7 ppm. This might give rise to an increase of the average global temperature because of the change in the atmos-pheric radiation budget - the so called greenhouse effect [10.41-42]. Ordinary air also contains widely varying amounts of water vapour. The gases N_2O, H_2, CH_4, NO_2, O_3, SO_2, CO, NH_3 etc. also are naturally present in the atmosphere in concentrations, that vary from several ppm to fractions of ppb (parts per billion). If such gases are found in higher concentrations in the air because of human activities they are considered as pollutants [10.43-47]. Measurements in the troposphere as well as in the stratosphere are of great interest. In the troposphere monitoring of industrial emissions as well as ambient air quality is needed for environmental protection purposes. Stratospheric measurements are important, e.g. for assessing possible long term changes in the absorption characteristics that could result in an altered radiation environment at the earth's surface (see also the discussion of possible ozone destruction, p.XXX). Further, laser technique also provide powerful means of remotely measuring meteorological conditions such as temperature, pressure, humidity, visibility and wind speed. We will discuss two active remote sensing techniques for the atmosphere - the long-path absorption technique and the lidar technique, but we will first consider a passive technique, in which lasers play an important part. The field of laser monitoring of the atmosphere is covered in several monographs and articles [10.48-53].

10.2.1 Optical heterodyne detection

Heterodyne detection is an important technique for low-noise signal recovery. Wellknown in the radio frequency region it has its counterpart also in the optical regime. The principle of optical heterodyne detection is given in Fig. 10.15. The incoming radiation is mixed in the detector with the radiation from a

Fig. 10.15 here

local oscillator, which could be a diode laser or a CO_2 laser. In the detector beats are generated at the difference frequency between the signal frequency ν_s and the local oscillator frequency ν_l. A narrow band electronic filter, that only transmits a fixed frequency ν_{if}, the intermediate frequency, selects the beat frequency $\nu_s - \nu_d = \nu_{if}$. ν_{if} is chosen in the radio frequency region

in which amplification easily can be performed. When the frequency of the local oscillator is swept the frequency of the recorded external signal is also swept and the spectrum will successively be recorded. The mixing of the signals can be described as

$$I = [A_s \sin(2\pi\nu_s t)+A_l \sin(2\pi\nu_l t)]^2 = A_s A_l \sin[2\pi(\nu_s-\nu_l)t] + \text{terms oscillating at high frequencies} \quad (10.4)$$

As we can see, the amplitude of the recorded signal is proportional to that of the incoming signal (A_s) as well as to that of the local oscillator (A_l). By increasing the amplitude of the local oscillator a noise-free amplification can be achieved. Heterodyne detection is frequently referred to as coherent detection. Sometimes it is convenient to also use a phase-sensitive (lock-in) detection at the frequency of a beam chopper for further increase of the signal-to-noise ratio and background rejection. In Fig. 10.16 an example of heterodyne detection is shown. The sun-disc is used as a radiation source and the absorption of the earth's atmosphere is monitored. The sun disc is tracked with a heliostat.

By tuning the local diode laser oscillator through the spectral region of an ozon infrared absorption line a signal with a pressure broadened component (See p.XXX) from the tropospheric ozon and a narrow component from the stratospheric layer (p.XXX) is recorded. By a mathematical deconvolution procedure the vertical ozon concentration profile can be calculated.

Fig. 10.16 here

10.2.2 Long path absorption techniques

The principle of long-path absorption techniques is shown in Fig. 10.17. A continuous laser beam is transmitted into the atmosphere

Fig. 10.17 here

against a corner-cube retro-reflector (p. xxx), that is placed at a distance of up to 10 km. The reflected beam is received by an optical telescope that is placed at the site of the laser and is directed towards the retro-reflector. The received light intensity is measured photo-electrically as a function of the laser wavelength. The absorption spectrum of the atmosphere between the laser and the retro-reflector is then recorded and the mean concentrations N_i of pollutant molecules can be determined using the Beer-Lambert relation.

$$\ln \frac{P_o(\nu)}{P_t(\nu)} 2R \left(\sum_{i=1}^{n} \sigma_i(\nu) N_i + K_{ext}\right) \quad (10.5)$$

Here $P_t(\nu)$ is the received light intensity and $P_o(\nu)$ is the intensity that would have been received in the absence of atmospheric absorption. $\sigma_i(\nu)$ is the absorption cross section for the molecules of the kind i. $\sigma_i(n)$ normally strongly varies with the wavelength while K_{ext} represents particle extinction that is largely wavelength independent in a small wavelength region. If several molecules absorb in the same wavelength range it is necessary to perform the measurements in a sufficiently large wavelength interval, preferably with a continously tunable laser to allow an unambigous determination of the individual molecular species. Frequently one tries to work in a wavelength region where the gas of interest is the dominant absorber. Then the measurement can convenintly be performed by rapidly switching the laser wavelength from the line center to a close-by off-line wavelength. Clearly, it is necessary to work in a wavelength region where the dominant atmospheric absorbers CO_2 and H_2O have a low absorption (See page XXX). Such regions can be found where the CO_2 and DF lasers emit, around 10 and 4 μm, respectively. These gas lasers are normally only line tunable and accidental wavelength coincidences are utilized. Sometimes two lasers, tuned to a resonance and an off-resonance frequently, respectively, are used and a rapid switching between transmission from the two lasers is performed. High-pressure CO_2 lasers and diode lasers are continously tunable. The long-path absorption technique is

mainly used for monitoring gases such as C_2H_4 (ethylene), C_2H_3Cl (vinyl cloride) O_3 and CO utilizing suitably located vibrational transitions. Results from a measurement of CO across a highway are shown in Fig 10.18.

Fig 10.18 here.

In a variant of the long-path absorption technique radiation from a diode laser or a light-emitting diode is transmitted fiber-optically to remotely located multi-pass absorption cells and the partially absorbed beam is sent back, also using fiber optics, to the measurement system. Using such a system which operates at short IR wavelength (1-2 μm), at which optical fibers transmit well, many points can be monitored form a central system with laser and computer facilities [10.54].

10.2.3 Lidar techniques

Lidar, which is an acronym for Light detection and ranging, is a measurement technique in which pulsed laser radiation is transmitted into the atmosphere and back-scattered light is detected at a certain time delay in a radar-like fashion. The principle of lidar (also called laser radar) is illustrated in Fig. 10.19. Laser light, that is back-scattered from a distance R arrives at the lidar receiver at a time delay t = 2R/c after the transmission of the pulse. The light velocity c is 300 m/μs. From the time delay range-resolved information can be obtained and the range-resolution ΔR is given by the duration of the laser pulse tp: $\Delta R = t_p c/2$. (Due to finite electronic response of the detection system the range resolution may be further impaired). The intensity of the received lidar signal is given by the general lidar equation:

$$R(R,\Delta R) = CWN_b(R)\sigma_b \frac{\Delta R}{R_2} \exp\left(-2\int_o^R (\sigma(\nu)N(r)+K_{ext}(r))\,dr\right) \qquad (10.6)$$

Fig. 10.19 here

W is the transmitted pulse energy and $N_b(R)$ is the number density of scattering objects with back-scattering cross section σ_b. The exponential factor describes the attenuation of the laser beam and the back-scattered radiation because of the presence of absorbing molecules of concentration N(r) and absorption cross section $\sigma(\nu)$, and due to attenuating particles with wavelength independent extinction coefficent K_{ext}. A single absorbing molecular specie is assumed. C is a system constant. The product $N_b(R)\sigma_b$ in the lidar equation determines the strength of the back-scattering which can be caused by several processes. It can be due to fluorescence from molecules that are resonantly excited by the laser light. At high pressures, i.e. in the troposphere, radiationless transitions due to collisions strongly quench the fluorescence light (See page xxx). On the other hand, fluorescence detection is very effient for monitoring of stratospheric constituents. In the stratosphere there are layers of Li, Na, K and Ca atoms at about 100 km height. These layers of atoms, that are produced mainly through evaporation of meteorites impinging into the atmosphere have very successfully been mapped out with ground-based fluorescence lidar systems operating with tunable dye lasers [10.55].

The backscattering can also be caused by the Raman process. Because of the weakness of this kind of scattering, high power laser beams are normally required even for monitoring of major atmospheric species. Here light backscattered with a characteristic Stokes frequency shift is detected. The technique has been used for vertical monitoring of water vapour profiles and for temperature measurements. Atmospheric visibility can also be assessed by measuring signals from N_2 molecules, that are recorded with reduced intensity because of mist and fog particles. Slant visibility measurements are of great interest, e.g. at airports.

The very strongest back-scattering process in the normal atmosphere is the Mie scattering against particles (See page XXX). Since the scattering is elastic, no information on the chemical composition of the particles is obtained. (Such information can be obtained using very high power laser pulses that through focusing can induce air break-down (laser sparks) at distances up

to 100 m. The emission spectrum from the spark carries information on vaporized particles [10.56]. The LIBS (Laser Induced Breakdown Spectroscopy) is also a powerful laboratory technique [10.57].) The intensity of the Mie-scattered light depends on the number density, size, shape, index of refraction and absorption properties of the particles [4.x.x]. Thus, a quantitative analysis requires a calibration, whereas relative particle spatial distributions can be obtained without large complications. Since the particle backscattering frequently strongly dominates over particle extinction K_{ext} the range-resolved lidar signal directly maps out the particle distribution $N_b(r)$.

The construction of a lidar system is illustrated in Fig. 10.20.

Fig. 10.20 here.

A Nd:YAG laser is used either directly or after frequency conversion in a dye laser to produce pulses that are transmitted into the atmosphere via a planar first-surface aluminized mirror. The same mirror is used for directing back-scattered light down into a fixed Newtonian telescope. In the focal plane of the telescope there is a polished metal mirror with a small hole, which defines the field-of-view of the telescope. For a telescope with a focal length of 1 m, a 1 mm hole corresponds to a telescope field-of-view of 1 mrad, which matches typical laser beam divergences. In order to suppress background light it is essential that the telescope only observes regions from which laser photons can be backscattered. The light passing the aparture is detected by a photomultiplier tube, whereas all the other light is directed into a TV camera, that produces a picture of the target area, except for the laser beam region which is seen as a black spot. The detected lidar signal is transferred to a transient digitizer (page XXX) and is read out to a computer system. The computer is used for controlling the planar mirror, the laser wavelength etc and also performs signal averaging and necessary processing of the lidar signals. In Fig. 10.21 particle monitoring with lidar techniques is illustrated. Increased back-scattering is monitored from particle plumes whereas a smoothly falling-off $1/R^2$ intensity is obtained from the uniform background particle distribution in the atmosphere.

Fig 10.21 here.

Fig. 10.22 here.

In order to measure the concentration of gaseous pollutants with lidar techniques, resonance absorption can be used in a similar way as in the long-path-absorption method that was described above. However, in the lidar technique no retro-reflector is required but the scattering from particles is utilized for generating a reflected signal. The particles serve as a "distributed mirror". The differential absorption at close-lying wavelengths of molecules in the atmosphere is used. The method, which is called dial (differential absorption lidar), is useful for qualitative as well as quantitative range-resolved measurements of air pollutants. The principles are illustrated in Fig. 10.22. For the sake of argument we consider an atmosphere with a uniform particle distribution and with two localized clouds of absorbing gas molecules. Lidar curves are recorded at a frequency of strong specific absorption ν_1 and at a closeby reference frequency ν_2. For atmosheres with typical particle size distributions, σ_b and K_{ext} will not change in the small frequency range, since the oscillatory behaviour, that is characteristic for uniform particles (page XXX), will be washed out. If particle extinction K_{ext} is small the recorded curves will for both frequencies have a simple $1/R^2$ dependence for the region preceeding the first gas cloud. For the non-absorbing frequency the lidar curve continues with a $1/R^2$ intensity fall-off even through the gas clouds, whereas intensity reductions occur in the on-resonance lidar curve at the site of the gas clouds. If no gas had been present both curves would have looked the same. The presence of an absorbing gas is best exhibited if the two curves are divided by each other as illustrated in the figure. Mathematically, this ratio can be formed by dividing the expressions for the lidar equation (10.6) for the two frequencies ν_1 and ν_2 :

$$\frac{P_{\nu_1}(R,\Delta R)}{P_{\nu_2}(R,\Delta R)} = \exp(-2(\sigma(\nu_1)-\sigma(\nu_2)) \int_0^R N(r)dr) \qquad (10.7)$$

As can be seen, all unknown parameters such as $N_b(r)$, σ_b and K_{ext} are eliminated at the division and only the absorption cross sections at the two frequencies have to be known from laboratory measurements for an evaluation of the gas concentration N(r) as a function of the distance R. We also realize that the method as a matter of fact not at all requires a uniform particle distribution, since any humps in the curves due to particle clouds would be divided away.

In Fig. 10.23 the absorption spectrum for SO_2 in the wavelength region around 300 nm is shown. In practical dial measurements of SO_2 the laser wavelength is changed between 300.05 nm and 299.30 nm every other laser pulse and the corresponding lidar curves are averaged in separate computer memories. An SO_2 measurement is illustrated in Fig. 10.24. Ozon can also be measured at wavelengths close to 300 nm, whereas NO_2 is monitored in the blue spectral region. Pollutants such as NO and Hg can be measured at short UV wavelengths, whereas CO, HF and hydrocarbons demand IR wavelengths. A review of atmospheric pollution monitoring using lidar techniques is given in Ref. [10.58].

Fig. 10.23 here.

Fig. 10.24 here.

It should be noted that the atmospheric back-scattering is considerable weaker at long wavelengths because of the strong wavelength dependence of Mie as well as Rayleigh scattering. In order to increase the signal-to-noise ratio of IR laser radar systems using e.g. pulsed TEA CO_2 lasers, heterodyne detection is frequently used (Section 10.1). Wind velocities can be remotely measured directly by frequency analyzing the beat between the back-scattered radiation that is Doppler shifted from moving particles and radiation from a CW laser tuned to the same frequency as the pulsed laser. Global wind field measurements as well as monitoring of molecules, especially O_3, are planned with space-borne lidar systems. Ground-based and air-borne lidar systems have been used in extensive studies of stratospheric dust particles following volcanic eruptions [10.59]. The particle contents of the atmosphere is important in considerations of the earths radiation balance. Meteorological parameters such as humidity, temperature and pressure can be measured with dial techniques using weak absorption lines of abundant species such as H_2O and O_2 in the red spectral region. Tunable solid state lasers such as alexandrite lasers (page XXX) are particularly suited for such measurements [10.60].

10.3 Laser-induced fluorescence and Raman spectroscopy in liquids and solids.

Laser-induced fluorescence (LIF) in liquids and solids can be used for diagnostic purposes in many contexts. Most substances have broad absorption bands in the UV region and a pulsed UV laser is frequently most useful for inducing fluorescence. The nitrogen laser (λ = 337 nm) is a simple and practical source in these contexts. Other useful laser systems are tripled Nd:YAG lasers (λ=355 nm) or excimer lasers (XeCl, λ=308 nm; KrF, λ=249 nm). Liquids and solids exhibit broad fluorescence emission bands [10.61-63]. As already discussed for dyes, sharp emission features are lost because of rotational quenching and mutual interactions between the molecules. Vibrational Raman spectra on the other hand exhibit quite sharp lines. Raman spectroscopy is a powerful tool for studing liquids and surface layers on solids. In this section we shall describe a few application of LIF and Raman spectroscopy of liquids and solids. We will first consider hydrosphere remote sensing and then discuss monitoring of surface layers.

10.3.1 Hydrospheric remote sensing

The increasing pollution of seas and inland waters calls for efficient methods for aquatic pollution monitoring. Oil spills cause very drastic damage to the environment. For marine monitoring, airborne surveillance systems are the most operational ones. All-weather capability generally calls for a microwave-based system. Fluorescence can be monitored at a distance with a modified lidar set-up and an airborne laser fluorosensor can be a valuable complement to a SLAR system (page XXX) for characterizing detected oil slick. Clearly, it is necessary to perform laboratory measurements of the substances of interest in order to

obtain the basic information necessary for an operational system. A laboratory set up for LIF studies is shown in Fig. 10.25. Either a scanning monochromator connected to a boxcar integrator is used, or better an optical multichannel analyzer (page XXX). In Fig. 10.26 LIF spectra for different substances in the aquatic environment are shown for N_2-laser excitation.

Fig. 10.25 here. Fig. 10.26 here.

A crude oil spectrum is shown featuring a broad and strong fluorescence spectrum. Oil products fluoresce quite strongly because of their contents of aromatic hydrocarbons such as antracene and naphtalene. Refined products fluoresce even stronger and with its peak fluorescence shifted to shorter wavelenghts, whereas heavy residual oils such as asphalt fluoresce weakly and mainly towards longer wavelengths. A spectrum of sea-water is also shown with a promient sharp signal due to the OH stretch Raman mode of H_2O. The broad blue fluorescence is due to organic water pollution. The spectrum also shows a fluorescence peak from a tracer dye that has been added to the water. Such dyes can be used to mark a "package" of water allowing studies of flow patterns in aquatic systems. A concentration as low as 1µg/l is sufficient for such fluorescence tracing. Included in Fig. 10.26 is also a spectrum from river water, polluted by lignine sulphonate from a pulp mill and a spectrum of water containing microscopic green algae. The prominent peak at 685 nm is due to the chlorophyll-a pigment, that is present in all plants [10.64]. LIF can be used for studying algal blooms in the sea and in lakes induced by eutrophication. Airborne oil monitoring systems have been constructed [10.65]. Oil slicks are detected by an increase of the blue fluorescence at the same time as the water Raman signal disappears because of full absorption in the oil layer.

Fig. 10.27 here

An airborne lidar system operating in the blue-green transmission window of water (page XXX) can be used for measurements of water depth [10.66]. The principle of such measurements is given in Fig. 10.27. The speed of light in water is about 0.75 c. Laser with a short pulse length must be used. Water is strongly attenuating and in order to enhance the weak bottom echo with respect to the strong surface echo a polarization scheme can be used. If the laser pulse is linearly polarized the surface echo remains largely polarized whereas the bottom echo is almost completely depolarized. Thus, by using a crossed linear polarizer in front of the detector a more reasonable relative strength of the two echoes is obtained. Depths down to several tens of meters can be measured by laser bathymeters of this construction. A frequency doubled Nd-YAG laser (λ=532 nm), a copper vapour laser (λ=510, 578 nm) or a HgBr laser (λ=520 nm) are candidates for laser bathymeters. Spaceborne green lasers are also being discussed for communication with submarines. The field of hydrospheric probing by lasers is discussed in Ref. [10.49].

10.3.2 Monitoring of surface layers

We have already mentioned that oils strongly absorb UV light. Thus, LIF can be used for detecting very thin surface layers of oil [10.67]. Industrially, it can be of interest of be able to establish that sheet metal components are free from oil before entering a painting shop. It is also interesting to monitor the presence of surface layers, e.g. of corrosion-protective agents. Examples of spectra of that kind are given in Fig. 10.28. Monitoring of the application of oil for rust protection during sheet metal coiling in a steel rolling mill using on industrial fluorosensor is illustrated in Fig. 10.29.

Fig. 10.28 here. Fig. 10.29 here.

The penetration depth in organic liquids rapidly increases for longer wavelengths. By chosing the proper excitation wavelength sensitive measurements of film thickness can be performed in different thickness ranges.

The fluorescence of organic substances can also be used for sensitive detection of signals in liquid chromatography [10.68]. Then a UV laser beam is used for exciting fluorescence at the outlet of the chromatography column. The varying wavelength distributions for different compounds can be used for further selectivly increase in complicated chromatography spectra.

Certain salts of rare earths exhibit sharp fluorescence lines when excited by UV light. It has been shown, that the relative strengths of different lines and also the decay time of the fluorescence at a certain fluorescence wavelength vary strongly with temperature. Thus, by applying thin layers of such salts on surfaces it is possible to remotely measure the temperature by LIF [10.69]. This technique could be particularly valable for hot rotating machine parts.

Surfaces of solids can also be investigated by Raman spectroscopy, which has a higher specificity than LIF [10.70]. Thus, this method is very suited for studying chemical processes such as corrision, electrochemical processes etc. Frequently, an Ar+ laser is used in conjunction with a double or triple monochrometer for isolating the Raman signals from the very strong elastic scattering from the surface. In Fig. 10.30 a Raman spectrum illustrating surface oxidation is shown.

Fig. 10.30 here.

The Raman scattering from a surface can be strongly enhanced as compared to the bulk material scattering. The enhancement is connected to periodic structures in the surface. Surface-enhanced Raman scattering is discussed in Ref. [10.71]. Surfaces can also be studied by other optical techniques. A method, in which the strength of surface frequency doubling of impinging laser light is investigated is rapidly evolving into a very powerful technique [10.72-73]. An example of surface studies by frequency doubling is shown in Fig. 10.31. The general field of laser spectroscopy of solids is covered in Ref. [10.74].

Fig. 10.31 here

10.4 Laser-induced chemical processes

Laser light can be used for inducing or controlling chemical processes in different ways. New possibilities in comparison to normal processes governed by thermodynamics thus arise. Photons of suitable energy can much increase the speed of a certain reaction leading to a strong increase in the yield of a desired substance. In this section we will discuss laser-induced chemical processes in general and also consider processes, in which a strong isotopic selectivity is obtained leading to laser isotope separation. The presently very active field to laser-induced processes is covered in a number of conference proceedings and reviews [10.75-79].

10.4.1 Laser-induced chemistry

A primary question in connection with laser-induced chemistry has been whether it would be possible to selectively break chemical bonds in large molecules by irradiating the molecules at a frequency corresponding to the vibrational mode associated with that particular bond. If this could be accomplished the possibilities to manipulate molecules would be almost inexhaustable. However, it turns out that the energy that is absorbed in a certain vibrational mode very quickly is distributed over the whole molecule. Therefore the excitation will be essentially thermal and unselective. In order to break a bond it is necessary to deposit a high energy in the bond in a time that must be less than 1 ps. This is technologically difficult. Thus, laser-induced chemistry instead has to rely on other processes.

By exciting a molecule to a higher vibrational level it can be made to react much faster (chemical activation). One example is the reaction

$$K + HCl \rightarrow KCl + H$$

This reaction occurs 100 times faster if the HCl molecules are excited to v = 1 as compared to v = 0. Laser radiation can also act as a catalyst in certain reactions, e.g. in the production of vinyl chloride C_2H_3Cl for the plastic industry. The process, which basically is a thermal break-up of dichlorethane C_2H_4Cl into C_2H_3Cl and HCl, can be run at considerably lower temperature in the presence of laser light. With an XeCl excimer laser (308 nm) free Cl radicals are formed that open up new reaction paths: Only one laser photon is needed for producing 10^4 vinyl chloride molecule since a chain reaction is utilized [10.80]. Laser radiation is also very effective in many pyrolysis reactions. Here a local heating of the reacting gases is accomplished by the laser light. As an example the cracking of heavy hydrocarbons into lighter ones can be mentioned. In the petrochemical industry it is frequently desirable to increase the yield of C_2H_4 over CH_4, since ethylene is a more desirable starting material for many petrochemical processes. Laser pyrolysis results in a higher yield than the one possible with thermal heating. Also for the production of ceramic materials, laser pyrolysis has a good potential. Using silane (SiH_4) as one starting product powders of Si, Si_3N_4 or SiC can be produced, later to be sintered into ceramics [10.79].

Laser chemistry can also be used for purifying certain chemicals. The production of ultrapure silicon for the semiconductor industry and for producing solar cells is of special interest. For optical fibers the purest possible SiO_2 is desirable. A suitable starting material is silane gas (SiH_4). Arsine, AsH_3, and phosphine, PH_3, are typical impurities. On radiation of the natural gas mixture with an ArF excimer laser (λ=193 nm) the impurities are quickly dissociated. The technique has a good production potential and the cost for purification could be quite reasonable. Since the cost of the laser photons always will be an important factor it is likely that laser-induced chemical processes will be advantageous especially for producing specialized and expensive chemicals, e.g. farmaceutics. Photoassisted production of vitamine D and prostaglandine has been considered [10.79].

10.4.2 Laser isotope separation

By using laser light of sharp frequency it is, utilizing the optical isotope shifts, possible to induce isotope selective processes leading to isotope separation. Enriched or separated isotopes are of great interest in many contexts. Pure radioisotopes are much used in medicine. Also stable elements such as ^{13}C can be used for studies of the metabolism and other biological processes. In NMR spectroscopy signals are only obtained from isotopes with a nuclear spin. For sulphur and calcium the useful isotopes ^{33}S and ^{43}Ca are naturally present only in very small concentrations. By using enriched isotopes in the building up of organic material completely new possibilities would open up. Enrichment of ^{14}C from organic objects that are to be dated would mean a much higher sensitivity since the tracer element could be concentrated into a small volume allowing small detectors to be used with a resulting low background count rate. In this way the time span when dealing with the ^{14}C method could be considerably increased.

However, the greatest interest for isotope separation comes from the nuclear power industry. Production of heavy water for heavy water reactors and separation of highly active components from the burnt out uranium fuel are two applications. The most important aspect by far is, however, isotope separation of ^{235}U. Natural uranium contains only 0.7 % of ^{235}U and an enrichment to about 3 % is needed for use in light water reactors. The normal separation method is diffusion of uranium hexafluoride UF_6 through porous filters. The process, which relies on the sligtly different mobility of $^{235}UF_6$ and $^{238}UF_6$, is very inefficient and the separation costs are very high and correspond to about 10 % of the resulting price for the produced electricity. Several nuclear reactors are needed for providing the electricity for a typical separation plant. A technique based on high-speed gas centrifuging is now being developed as a possible alternative. At the same time laser techniques for uranium isotope separation are being investigated in several countries. Clearly, any technique

that could reduce the separation costs would be of great interest. Laser techniques can lead to high degree of enrichment and may be useful also in processing of uranium tailings form which most of the fissile material has already been removed.

Laser isotope separation schemes based on free atoms or on UF_6 are possible. In both cases the presence of an isotope shift is critically utilized. We will first consider free atoms. For heavy element such as uranium the isotope shift is only due to the volume effect (page XXX). In Fig. 10.32 the different isotopically separated components of a uranium emission line are shown for an enriched sample. The broadening in the ^{235}U line is due to unresolved hyperfine structure. The basic principle for atomic uranium separation is shown in Fig. 10.33.

Fig 10.32 here. Fig. 10.33 here.

A narrow-band tunable laser selectively transfers ^{235}U atoms to an excited state. Since atomic transitions can be saturated with laser pulses (page XXX) a large fraction of the ^{235}U atoms are transferred to the higher state from which they can be photo-ionized using a second laser pulse. The photon energy for this laser is not sufficient for photo-ionizing ground-state atoms. The ^{235}U ions that in this way have been formed, are extracted to a collector plate using an electric field. A separation scheme with two selective excitation steps induced by dye lasers that are pumped by powerful copper vapour lasers is being explored for practical separtion purposes. A powerful excimer laser is used for the photo-ionizing step. The properties of uranium call for special evaporation techniques. It is necessary to heat the uranium to 2300 K for achieving a substantial evaporation. However, molten uranium metal is extremely reactive and attacs most oven materials. One technique to overcome this problem is to use local surface heating with electron guns.

Uranium isotope separation using a molecular approach is based on selective multi-photon dissocation of UF_6. The relevant vibrational isotope shift is 0.6 cm^{-1} in the primary vibrational transition at 628 cm^{-1} (16μm). In the development of the technique, experiments on SF_6 have been very important. The conditions are much more favourable for SF_6 than for UF_6. The isotope shift is 17 cm^{-1} between ^{32}S and ^{34}S in the IR active vibrational mode that involves assymetric streching of two S-F bands. The spectrum has a typical P, Q and R-branch structure and the whole region of absorption for the rotational level population distribution that is obtained at room temperature is 15 cm^{-1}. Thus, the isotopic molecules are spectroscopically totally separated. Further, the vibrational transition in $^{32}SF_6$ well matches the emission of a free-running pulsed CO_2 laser.

The multi-photon dissociation process is illustrated in Fig. 10.34. Because of the anharmonicity of the vibrational potential

Fig. 10.34 here.

a photon energy that is resonant in the first vibrational step will successively pull out of resonance higher up in the vibrational energy level ladder. Still the molecule can be excited in a multi-photon process (page XXX) until it is dissocated (page XXX). SF_6 then disintegrates into SF_5 and F. By making the first step resonant for one isotopic molecule the probability for subsequent dissociation for this molecular specie is drastically increased.

The corresponding process for UF_6 has as a prerequisite the availability of efficient lasers in the 16 μm region. This has spurred a considerable effort in accomplishing such lasers. An efficient way to generate laser radiation at 16 μm is to Raman shift a pulsed CO_2 laser at 10.6 μm. By stimulated Raman scattering in a multi-pass cell filled with para -H_2 a 16 μm beam can be produced at a 50 % efficiency. Rotational transitions in this molecule with parallel nuclear spins are used. A problem with UF_6 is that the width of the sharpest feature in the spectrum (the Q-branch) is 5 cm^{-1} at room temperature, which much exceeds the isotope shift. Thus the selectivity is poor. By using two CO_2 laser wavelengths in the 16 μm region the selectivity can be increased. By a dynamic cooling of the UF_6 gas through expansion from a super-sonic nozzle the number of populated rotational levels can be drastically reduced leading to a much better resolution of the Q-branches of the two isotopic molecules. Even

then two separate 16 μm wavelengths are favourable and further efficiency is gained by adding excimer laser UV photons for more efficient photo-dissociation of molecules that are excited in the multi-photon process. At the UF_6 dissociation, UF_5 molecules are formed, constituting a powder, that can be collected.

For separation of ^{13}C, multi-photon dissocation of Freon-22 (CF_2HCl) or CF_3I can be used and macroscopic quantities are being produced utilizing CO_2 TEA lasers. Heavy water (D_2O) can also be enriched with a multiphoton process utilizing CO_2 laser radiation acting on CF_3D molecules:

$$CF_3D \xrightarrow{nh\nu} CF_2 + DF$$

$$2DF + CaO \rightarrow D_2O + CaF_2$$

The isotope shift between CF_3D and CF_3H is large and the cross sections for multi-photon absorption differ by a factor of 6000 between the two molecules.

Formaldehyde, HCHO, has also been studied much. Using multi-photon processes this molecule can be used for separation of hydrogen, carbon as well as oxygen.

Step-wise processes involving few photons can also be used for molecules. As a matter of fact one of the first laser separations was performed in this way. This experiment on NH_3 molecules is illustrated in Figs. 10.35 and 10.36.

Fig. 10.35 here. Fig. 10.36 here.

A mixture of $^{14}NH_3$ and $^{15}NH_3$ is kept in a cell and is irradiated by a pulsed CO_2 laser which only can excite $^{14}NH_3$ vibrationally because of the isotope shift. At the same time a strong UV source consisting of a spark discharge in air is fired. The UV photons dissociate the vibrationally excited molecules but because of proper filtering no photons with sufficient energy to dissociate ground-state molecules are available. The following reactions occur, but only for $^{14}NH_3$:

$$NH_3 + h\nu \rightarrow NH_2 + H$$

$$NH_2 + NH_2 \rightarrow N_2H_4$$

$$N_2H_4 + H \rightarrow H_2H_3 + H_2$$

$$2N_2H_3 \rightarrow 2NH_3 + N_2$$

Thus, isotopically enriched $^{14}N_2$ gas has been formed in the cell. Similar processes can be used for boron and chlorine separation.

For production of clean radio isotopes for medical use it is favourable to induce the nuclear reactions in the properly chosen isotopically pure elements. Examples of such processes are:

$^{203}Tl \rightarrow {}^{201}Tl$, $^{124}Te \rightarrow {}^{123}I$, $^{68}Zn \rightarrow {}^{67}Ga$ and $^{190}Os \rightarrow {}^{191}Ir$.

The annual world demand for such isotopes might be of the order of 100 grams but since conventional production schemes are extremely costly, laser isotope separation might here be an attractive possibility.

10.5 Spectroscopic aspects of lasers in medicine

Lasers are finding increasing applications in the field of medicine. Normally the heating effect of laser beams is utilized. At a temperature rise from 37° to 44°C the enzymatic and electrical activties of the cells are disrupted. At 60°C protein denaturation occurs and at 100°C the cells rupture due to the boiling of the cellular fluid. Carbonization occurs of temperatures above 200°C. The laser power densities required to attain a certain temperature rise clearly depends on the absorption properties of the tissue, which are much governed by the properties of water and hemoglobine. Skin absorption is largely due to melanine. The corresponding absorption curves are included in Fig. 10.37.

Fig. 10.37 here. Fig. 10.38 here.

Beams from the three most important medical laser types, the CO_2, the Nd:YAG and the Ar+ -laser have a surgical penetration depth of about 0.1 mm, 4 mm and 1 mm, respectively in normal tissue. Short-wavelength excimer lasers have a very low penetration depth and tissue removal is caused by ablation. Under the pulsed irradiation the tissue is lifted off layer by layer. These lasers are now being extensively investigated for medical use.

An important feature of laser beams in surgery is their ability to cut and at the same time coagulate the blood vessels, which strongly reduces the need for blood transfusions ("the blood-less knife"). The thickness of the coagulated zone varies with the laser wavelength used. Other advantages are the sterile, non-touching nature of the cutting and the minimum mechanical strain on the tissue. The last point is particularly important in neurosurgery. Lasers are also used for vapourizing tumours. The laser radiation from Nd:YAG and Ar+ lasers can conveniently be delivered through flexible optical fibers that are highly transparant to the corresponding wavelengths. However, for CO_2 no fibers have been available until very recently, when first fibers of limited applicability appeared. Normally, CO_2 radiation is delivered through a specially designed multi-joint arm that is terminated with a handpiece.

The strong absorption of green Ar+ radiation in blood can be utilized for selective coagulation of small blood vessels. This is utilized in the treatment of portwine stains. This dermatological disease is caused by excessive growth of a network of tiny blood vessels close to the skin. The laser light penetrates the skin but is absorbed in the blood eliminating the cause of skin discolouration.

Ar+-lasers are also used for photo coagulation treatment of excessive blood vessel growth in the retina of diabetes patients. It is also used for "spotwelding" of the retina in the case of retinal detachment. Because of the relatively easy optical access to the interior of the eye this organ is well suited for laser treatment. The absorption characteristics of different parts of the eye are given in Fig. 10.38. The retina consists of many layers with different absorption properties. Thus by choosing the

wavelength an energy dose can be delivered to a particular layer with a certain selectivity. One area in the retina has very special absorption properties because of its high contents of xantophyll. The optical and spectroscopic properties of the eye largely determine the criteria for safe utilization of lasers and form the basis for legal classification of lasers. The US regulations [10.81] are frequently used as a starting point in setting up national rules. The maximum permissible dose of laser light for eye exposure obviously varies strongly with wavelength. The strictest regulations apply for the wavelength region 400 -1XXX nm, in which the retina is fully exposed to the radiation. As a matter of fact, the Nd:YAG laser operating at 1.06 μm is one of the most dangerous lasers from an eye safety point of view since it penetrates into the eye, yet the presence of beams is not revealed through scattering, since the wavelength falls in the invisible region. For wavelengths below 400 nm absorption occurs in the cornea. However, high doses of UV absorbed in the cornea cause cataracts. The most relaxed regulations pertain to the wavelength region above 1.X μm where only the heat deposition in the cornea sets the limit. For detailed accounts of the medical use of the thermal energy in laser beams we refer to [10.82-10.85].

Apart from the surgical application of laser beams discussed above, a new interesting field of laser utilization for tumour localization and treatment is emerging. The techniques take advantage of the special properties of certain agents, most notably hematoporphyrin derivative (HPD) [10.85-91]. After intravenous injection (typically at 3 mg/kg bodyweight), the HPD molecules are distributed all over the body. However, after a few days the material is excreted from the body, but not from tumours, where it is selectively retained as illustrated in Fig. 10.39.

Fig. 10.39 here. Fig. 10.40 here.

Whereas the HPD molecules themselves have no therapeutic effect they have two important properties that can be used in connection with the selective retention just mentioned. The molecules have a very characteristic dual-peaked fluorescence in the red spectral

region as illustrated in Fig. 10.40. The excitation is most efficiently performed in the Soret band peaking at 405 nm. The violet lines of a Kr+ laser (page XXX) falls conveniently in this region, but Ar+ laser lines or the N_2 laser emission can also be used. The fluorescence can be utilized for localizing tumours [10.92-95], e.g. in the lung or bladder, that would otherwise not be visible in normal endoscopic investigations with viewing devices based on fiber optics. The other important property of HPD is that upon excitation and subsequent transfer to its triplet state, 3π, the HPD molecules can transfer their excitation energy to ground state 3Σ oxygen molecules that are present in the tissue as indicated in Fig. 10.39. The oxygen molecules are then excited from the triplet state to a singlet state. Singlet oxygen is known to strongly react with tissue through rapid oxidation and the tissue becomes necrotic. The process is thus of the laser-induced chemistry type (page XXX) and involves heating of the tissue only as a weak secondary effect. Since the process only occurs in the presence of HPD and HPD is accumulated in tumours a selective therapy is obtained. Again, the HPD excitation most efficiently takes place in the Soret band. However, normally the absorption peak of HPD at 630 nm is preferred since tissue transmits this radiation much better because the wavelength falls outside the region of strong hemoglobine absorption. (See Fig. 10.36.) An effective penetration depth of about 1 cm is achieved. CW argon-ion or a pulsed copper vapour laser pumping a dye laser is used for generating the 630 nm radiation but the 628 nm emission from a pulsed gold vapour laser can also be utilized. The laser radiation can conveniently be delivered through a quartz optical fiber. For superficial tumours the radiation is applied directly on the surface and doses of tens of J/cm^2 are normally used. The radiation can also be fiber-optically delivered through a bronchoscope or a cystoscope for lung and bladder applications, respectively. For deep-lying lesions the laser light can be transmitted fiber-optically through the lumen of a syringe needle that is inserted into the tumour mass. A remarkable rate of success has been reported for this new type of treatment which is normally referred to as HPD-PDT (Hematoporphyrin Derivative - Photo-Dynamic Therapy). New

photosensitizers are being investigated. Ptalocyanine has the attractive property of absorbing laser radiation at about 700 nm where the tissue penetration depth is much increased (see Fig. 10.37).

We will end this section by further discussing fluorescence diagnostics techniques for tissue, since the techniques have a wide applicability also in other areas. Clearly, practical monitoring of HPD containing tissue has to address the problems of how to deal with background signals, that tend to obscure the specific signal. In Fig. 10.41 spectra from a superficial tumour

Fig. 10.41 here.

and surrounding muscle from a HPD-injected rat are shown. A nitrogen laser at 337 nm was used for the excitation and the fluorescence spectra were recorded with an optical multichannel analyzer (page XXX). In the upper part of the figure the details from a tumour spectrum are shown with the characteristic dual-peaked HPD emission sitting on the slope of the strong blue natural tissue fluorescence. Below spectra that are recorded at different locations along a line extending from normal muscle into cancer tumour are shown. The signal intensities as defined in the top figure are also evaluated. It can be seen that the blue fluorescence intensity B decreases in the tumour tissue. The background free HPD signal A at 630 nm clearly increases in the tumour whereas the signal A' which incluces the background varies only little. By forming the ratio A/B contrast is strongly enhanced between normal and malignant tissue. We note that monitoring of a dimensionless quantity has many advantages. Temporal or spatial variations in the exciting radiation will not influence the result. The ratio is also insensitive to the surface topography, i.e. the signal is not influenced by the angles of incidence and detection but only responds to changes in the specific spectral signature. These concepts are valuable for imaging fluorescence measurement techniques, that can be applied for medical as well as for industrial and remote-sensing applications [10.96].

Differences in the natural fluorescence (autofluorescence) of various tissues can also be utilized for diagnostics [10.97-10.98]. Thus, tissue autofluorescence has been used for tumour characterization [10.99-101] as well as for caries studies in tumours teeth [10.102-103]. An emerging application is characterization of artherosclerosis in blood vessels [10.104]. Fluorescence diagnostics would be particularly valuable for guiding laser removal of artherosclerotic plaque [10.105-106].

Time-resolved fluorescence spectroscopy is also a valuable tool in biological and medical research [10.107-108]. Since the lifetimes involved are normally short, pico-second spectroscopy techniques are frequently employed (p. xxx].

REFERENCES, CHAPTER 10

10.1 M. Gehring, K. Hoyermann, H. Schacke, J. Wolfrum: Direct Studies of some Elementary Steps for the Formation and Destruction of Nitric Oxide in the H-N-O System, 14th Symposium on Combustion (Combustion Institute, 1973)

10.2 W.C. Gardiner, Jr.: The Chemistry of Flames, Sci. Amer. 246, 110 (1982)

10.3 A. G. Gaydon, H. G. Wolfhard: Flames, their Structure, Radiation and Temperature (Chapman and Hall, New York 1979)

10.4 A. C. Gaydon: The Spectroscopy of Flames (Chapman and Hall, New York 1974)

10.5 D.R. Crosley (ed.): Laser Probes for Combustion Chemistry (Amer. Chem. Soc., Washington 1980)

10.6 A.C. Eckbreth, P.A. Bonczyk, J.F. Verdiek: Progress in Energy and Combustion Science 5, 253 (1979).

10.7 J.H. Bechtel, A.R. Chraplyvy: Proc. IEEE 70, 658 (1982)

10.8 J. Wolfrum: Chemical Kinetics in Combustion Systems: The Specific Effect of Energy, Collisions, and Transport Processes, 20th Symposium on Combustion (Combustion Institute, Pittsburg 1985)

10.9 N.S. Bergano, P.A. Janimaagi, M.M. Salour, J.H. Bechtel: Opt. Lett. 88, 443 (1983)

10.10 M. Aldén, H. Edner, G. Holmstedt, S. Svanberg, T. Högberg: Single-Pulse Laser-Induced OH Fluorescence in an Atmospheric Flame, Spatially Resolved with a Diode Array Detector, Appl. Opt. 21, 1236 (1982); M.J. Dyer, D.R. Crosley: Two-Dimensional Imaging of OH Laser-Induced Fluorescence in a Flame, Opt. Lett. 7, 382 (1982); G. Kychakoff, R.D. Howe, R.K. Hanson, J.C. McDaniel: Quantitative Visualization of Combustion Species in a Plane, Appl. Opt. 21, 3225 (1982)

10.11 G. Kychakoff, R.D. Howe, R.K. Hanson: Appl. Opt. 23, 704 (1984); G. Kychakoff, K. Knapp, R.D. Howe, R.K. Hanson: AIAA J. 22, 153 (1984)

10.12 R.P. Lucht, J.P. Salmon, G.B. King, D.W. Sweeney, N.M. Laurendeau: Opt. Lett. 8, 365 (1983); P.J.H. Tjossem, T.A. Cool: Chem. Phys. Lett. 100, 479 (1983).

10.13 M. Aldén, S. Wallin, W. Wendt: Appl. Phys. B33, 205 (1984)

10.14 J.E.M. Goldsmith: Opt. Lett. 7, 437 (1982)

10.15 K. Tennel, G.J. Salomo, R. Gupta: Appl. Opt. 21, 2133 (1982)

10.16 S.M. Schoenung, R.K. Hanson: Comb. Sci. Techn. 24, 227 (1981); K. Knapp, R.K. Hanson: Appl. Opt. 22, 1980 (1983)

10.17 Proc. IEEE 71, 291-435 (1983)

10.18 K.E. Bennett, G.W. Faris, R.L. Byer: Experimental Optical Fan Beam Tomography, Appl. Opt. 23, 2678 (1984); H.M. Hertz: Experimental Determination of 2-D Flame Temperature Fields by Interferometric Tomography, Opt. Commun. 54, 131 (1985)

10.19 A. Rose, G.J. Salamo, R. Gupta: Appl. Opt. 23, 781 (1984); H. Sonntag, A.C. Tam: Opt. Lett. 10, 436 (1985)

10.20 M. Lapp, C.M. Penney: Raman Measurements on Flames, in R.J.H. Clark, R.E. Hester (eds.), Advances in Infrared and Raman Spectroscopy (Heyden & Sons 1977)

10.21 M. Aldén, S. Wallin: CARS Experiment in a Full-Scale (10 x 10 m²) Industrial Coal Furnace, Appl. Opt. 24, 3434 (1985)

10.22 B. Attal, M.Pealat, J.P. Taran: J. Energy 4, 135 (1980)

10.23 A.C. Eckbreth, P.W. Schreiber: Coherent anti-Stokes Raman Spectroscopy (CARS): Applications to Combustion and Gas-Phase Diagnostics, in A.B. Harvey (ed.): Chemical Applications of Noi-Linear Raman Spectroscopy (Academic Press 1981)

10.24 M. Aldén, H. Edner, S. Svanberg: Coherent Anti-Stokes Raman Spectroscopy (CARS) Applied in Combustion Probing, Phys. Scripta 27, 29 (1983)

10.25 H. Haragushi, B. Smith, S. Weeks, D.J. Johnson, J.D. Wineforder: Measurement of Small Volume Flame Temperature by the Two-Line Atomic Fluorescence Method, Appl. Spectr. 31, 156 (1977); R.G. Jolik, J.W. Daily: Two-Line Atomic Fluorescence Temperature Measurements in Flames: An Experimental Study, Appl. Opt. 21, 4158 (1982); M. Aldén, P. Grafström, H. Lundberg, S. Svanberg: Spatially Resolved Temperature Measurements in a Flame using Laser-Excited Two-Line Atomic Fluorescence and Diode-Array Detection, Opt. Lett. 8, 241 (1983)

10.26 Sparks, Ignition

10.27 T.R. Evans (ed.): Applications of Lasers to Chemical Problems (Wiley, New York 1982)

10.28 K.L. Kompa, J. Wanner: Laser Applications in Chemistry (Plenum Press, New York 1984); V.S. Letokhov (ed.): Laser Analytical Spectrochemistry, Adam Hilger Series on Optics and Optoelectronics (Adam Hilger, Bristol 1986)

10.29 R.M. Osgood, S.R.J. Brueck, H.R. Schlossberg (eds.): Laser Diagnostics and Photochemical Processing for Semiconductor Devices (North Holland, Amsterdam 1983)

10.30 D. Bäurle (ed.): Laser Processing and Diagnostics, Springer Series in Chemical Physics, Vol. 39 (Springer, Berlin, Heidelberg, New York 1984)

10.31 E.R. Pike, H.Z. Cummins (eds.): Photon Correlation and Light Beating Spectroscopy (Plenum Press, New York 1974)

10.32 L.E. Drain: The Laser Doppler Technique (John Wiley, Chichester 1980)

10.33 E. Durst, A. Melling, J.H. Whitelaw: Principles and Practice of Laser-Doppler Anemometry, 2nd Ed. (Academic Press, London 1981)

10.34 C. Dasch; R. Miles; Tagging

10.35 B. Hiller, J.C. McDaniel, E.C. Rea, Jr., R.K. Hanson: Opt. Lett. 8, 474 (1983); U. Westblom, S. Svanberg: Imaging Measurements of Flow Velocitites using Laser-Induced Fluorescence, Phys. Scripta 31, 402 (1985)

10.36 M. Alden, H. Edner, P. Grafström, H.M. Hertz, G. Holmstedt, T. Högberg, H. Lundberg, S. Svanberg, S. Wallin, W. Wendt, U. Westblom: Imaging Measurements of Species Concentrations, Temperatures and Velocities in Reactive Flows using Laser-Induced Fluorescence, Lasers 86, p. 219 (STS Press, McLean, Va. 1985)

10.37 R.K. Hanson: Review of Imaging

10.38 E.J. McCartney: Absorption and Emission by Atmospheric Gases (Wiley, New York 1983)

10.39 L.S. Rothman: AFGL Spectral Tape, Appl. Opt. 22, 2247 (1983)

10.40 E.J. McCartney: Optics of the Atmosphere; Scattering by Molecules and Particles (Wiley, New York 19..)

10.41 W. Bach, J. Pankrath, W. Kellogg (eds): Man's Inpact on Climate (Elsevier, Amsterdam 1979)

10.42 R. Revelle: Carbon Dioxide and World Climate, Sci. Amer. 247, No. x, 35 (1982)

10.43 T.E. Graedel, D.T. Hawkins, L.D. Claxton: Atmospheric Chemical Compounds: Sources, Occurrence, Bioassay (Academic Press, Orlando 1986)

10.44 R.M. Harrison, R. Perry (eds.): Handbook of Air Pollution Analysis, 2nd Ed. (Chapman and Hall, London 1986)

10.45 R.P. Wayne: Chemistry of Atmospheres (Clarendon Press, Oxford 1985)

10.46 J.H. Seinfeld: Atmospheric Chemistry and Physics of Air Pollution (Wiley, New York 1986)

10.47 M.R. Rampino, S. Self: The Atmospheric Effects of El Chichon, Sci. Amer. 280, 48 (1984)

10.48 D.A. Killinger, A. Mooradian (eds.): Optical and Laser Remote Sensing, Springer Series in Optical Sciences Vol. 39 (Springer, Berlin, Heidelberg, New York 1983)

10.49 R.M. Measures: Laser Remote Sensing: Fundamentals and Applications (Wiley, New York 1984)

10.50 R.M. Measures, in N. Omenetto (ed.): Analytical Laser Spectroscopy (John Wiley, New York 1979) ?

10.51 E.D. Hinkley (ed.): Laser Monitoring of the Atmosphere, Topics in Applied Physics, vol. 14 (Springer, Berlin, Heidelberg, New York 1976)

10.52 V. Zuev, I. Naats: Inverse Problems of Lidar Sensing of the Atmosphere, Springer Series in Optical Sciences, Vol. 29 (Springer, Berlin, Heidelberg, New York 1983)

10.53 S. Svanberg: Lasers as Probes for Air and Sea, Contemp. Phys. 21, 541 (1980); S. Svanberg: Fundamentals of Atmospheric Spectroscopy, in T. Lund (ed.): Surveillance of Environmental Pollution and Resources by Electromagnetic Waves (D. Reidel, Dordrecht 1978)

10.54 H. Inaba, Fibre spectroscopic network

10.55 G. Megie, Stratospheric Atomic Species Monitoring

10.56 V. Zuev, Remote Laser-Induced Breakdown Spectroscopy, Proc. Laser Radar Conference, Aix-en-Provence

10.57 L. Radziemski: Laser-Induced Breakdown Spectroscopy

10.58 K.A. Fredriksson, Review of Differential Absorption Lidar, in R.M. Measures (ed.), to appear

10.59 Mc Cormick, Stratospheric Dust Probing by Lidar

10.60 Refs 8.53-54

10.61 D.H. Hercules (ed.): Fluorescence and Phosphorsence Analysis (Interscience Publ., New York 1966)

10.62 J.B. Birks: Photophysics of Aromatic Molecules (Wiley, New York 1970)

10.63 I. Berlman: Handbook of Fluorescence Spectra of Aromatic Molecules, 2nd Ed. (Academic Press, New York 1971)

10.64 Govindjee, R. Govindjee: The Absorption of Light in Photosynthesis, Sci. Amer. 231, Nr ,68 (1974); F.E. Hoge, R.N. Swift: Airborne Simultaneous Spectroscopic Detection of Laser-Induced Water Raman Backscatter and Fluorescence from Chlorophyll a and Other Naturally Occuring Pigments, Appl. Opt. 20, 3197 (1981); F.E. Hoge, R.N. Swift, J.K. Yungel: Active-Passive Airborne Ocean Color Measurement. 2: Applications, Appl. Opt. 25, 48 (1986)

10.65 R.A. O'Neill, L. Buja-Bijunas, D.M. Rayner: Field Performance of a Laser Fluorosensor for the Detection of Oil Spills, Appl. Opt. 19, 863 (1980); G.A. Capelle, L.A. Franks, D.A. Jessup: Aerial Testing of a KrF Laser-Based Fluorosensor, Appl. Opt. 22, 3382 (1983)

10.66 H.H. Kim: Airborne Laser Bathymetry

10.67 S. Montán, S. Svanberg: A System for Industrial Surface Monitoring Utilizing Laser-Induced Fluorescence, Appl. Phys. B38, 241 (1985); S. Montán, S. Svanberg: Industrial Applications of Laser-Induced Fluorescence, L.I.A. ICALEO 47, 153 (1985)

10.68 Liquid Chromatography with LIF Detection

10.69 J.S. McCormack: Remote Optical Measurements of Temperature Using Fluorescent Materials, Electr. Lett. 17, 630 (1981); A.F. Cheng: Fluoroptic Thermometry, Measurement and Control News (April 1984)

10.70 Surface Raman Analysis

10.71 SER spectroscopy

10.72 Y.R. Shen: Surface frequency doubling

10.73 Surface studies with lasers

10.74 Yen (ed.): Solids

10.75 V.S. Letokhov: Non-Linear Laser Chemistry, Springer Series in Chemical Physics Vol. 22 (Springer, Berlin, Heidelberg, New York 1983)

10.76 E. Grunvald, D.F. Dever, P.M. Keeher (?): Megavatt Infrared Laser Chemistry (Wiley, New York 1978)

10.77 Zewail et al (eds.):

10.78 Photophysics and Photochemistry above 6 eV (Elsvier Science Publ., Amsterdam 1985)

10.79 Applications of Lasers to Industrial Chemistry, SPIE Vol. 456 (SPIE, 1984)

10.80 P.N. Clough, M. Kneba, M. Schneider, J. Wolfrum: European Patent Application No. 801056490.

10.81 ANSI

10.82 L. Goldman (ed.): The Biomedical Laser: Technology and Clinical Applications (Springer, Berlin, Heidelberg, New York 1981)

10.83 J.-L. Boulnois: Photophysical Processes in Recent Medical Laser Developments: a Review, Lasers in Med. Sci. 1, 47 (1986)

10.84 J.-L. Boulnois, in ....

10.85 J.A. Parrish, T.F. Deutsch: Laser Photomedicine, IEEE J. Quant. Electr. QE-20, 1386 (1984).

10.86 T.J. Dougherty: in CRC Critical Reviews in Oncology/ Hematology, S. Davis (ed.) (CRC, Boca Raton 1984)

10.87 Y. Hayata, T.J. Dougherty (eds.): HPD Monograph

10.88 R. Pratesi, C.A. Sacchi (eds.): Lasers in Photomedicine and Photobiology (Conf. Proc.), Springer Series in Optical Sciences Vol. 22 (Springer, Berlin, Heidelberg, New York 1980)

10.89 A. Andreoni, R. Cubeddu (eds.): Porphyrins in Tumor Phototherapy (Plenum Press, New York 1984)

10.90 Y. Hayata (ed.): Proceedings of the First International Conference on the Application of Photosensitization for Diagnosis and Treatment, Tokyo 1986, in press.

10.91 Ch.J. Gomer (ed.): Proc. of the Clayton Foundation Conference on Photodynamic Therapy (Childrens Hospital, Los Angeles 1987)

10.92 A.E. Profio, D.R. Doiron, O.J. Balchum, G.C. Huth: Fluorescence Bronchoscopy for Localization of Carcinoma in Situ, Med. Phys. 10, 35 (1983)

10.93 H. Cato, D.A. Cortese: Early Detection of Lung Cancer by means of Hematoporphyrin Derivative Fluorescence and Laser Photoradiation, Clinics in Chest Medicine 6, 237 (1985)

10.94 J.H. Kinsey, D.A. Cortese: Rev. Sci. Instr. 51, 1403 (1980)

10.95 S. Svanberg: Tissue Diagnostics using Laser-Induced Fluorescence, Physica Scr., to appear

10.96 P.S. Andersson, S. Montán, S. Svanberg: Multi-Spectral System for Medical Fluorescence Imaging, IEEE J. Quant. Electr., in press

10.97 S. Udenfriend: Fluorescence Assay in Biology and Medicine, Vol. I (1962), Vol. II (1969) (Academic Press, New York)

10.98 G.M. Barenboim, A.N. Domanskii, K.K. Turoverov: Luminescence of Biopolymers and Cells, (Plenum Press, New York 1969)

10.99 Y.M. Ye, Y.L. Yang, Y.F. Li, F.M. Li: Characteristic Autofluorescence for Cancer Diagnosis and the Exploration of its Origin, Proc. CLEO'85 Conference, Baltimore, USA

10.100 R.R. Alfano, B.T. Darayash, J. Cordero, P. Tomashefsky, F.W. Longo, M.A. Alfano: Laser Induced Fluorescence Spectroscopy from Native Cancerous and Normal Tissue, IEEE J. Quant. Electr. QE-20, 1507 (1984)

10.101 P.S. Andersson, E. Kjellén, S. Montán, K. Svanberg, S. Svanberg: Autofluorescence of Various Rodent Tissues and Human Skin Tumour Samples, Lasers in Medicine, in press

10.102 R.R Alfano, W. Lam, H.J. Zarrabi, M.A. Alfano, J. Cordero, D.B. Tata, C.E. Swenberg: Human Teeth with and without Caries Studied by Laser Scattering, Fluorescence and Absorption Spectroscopy, IEEE J. Quant. Electr. QE-20, 1512 (1984).

10.103 F. Sundström, K. Fredriksson, S. Montán, U. Hafström-Björkman, J. Ström: Laser-Induced Fluorescence From Sound and Carious Tooth Substance: Spectroscopic Studies, Swed. Dent. J. 9, 71 (1985)

10.104 C. Kittrell, R.L. Willett, C. de los Santon-Pacheo, N.B. Ratliff, J.R. Kramer, E.G. Malk, M.S. Feld: Diagnosis of Fibrous Arterial Atherosclerosis Using Fluorescence, Appl. Opt. 24, 2260 (1985)

10.105 J.M. Isner, R.H. Clarke: The Current Status of Lasers in the Treatment of Cardiovascular Disease, IEEE J. Quant. Electr. QE-20, 1406 (1984).

10.106 M.R. Prince, T.F. Deutsch, M.M. Matheve-Roth, R. Margolis, J.A. Parrish, A.R. Oseroff: Preferential Light Absorption in Atheromas in Vitro: Inplications for Laser Angioplasty, J. Clin. Invest. 76, 295 (1986).

10.107 S.R. Meech, C.D. Stubbs, D. Phillips: The Application of Fluorescence Decay Measurements in Studies of Biological Systems, IEEE J. Quant. Electr. QE-20, 1343 (1984).

10.108 M Yamashita, M. Nomura, S. Kobayashi, T. Sato, K. Aizawa: Picosecond Time-Resolved Fluorescence Spectroscopy of Hematoporphyrin Derivative, IEEE J. Quant. Electr. QE-20, 1383 (1984)

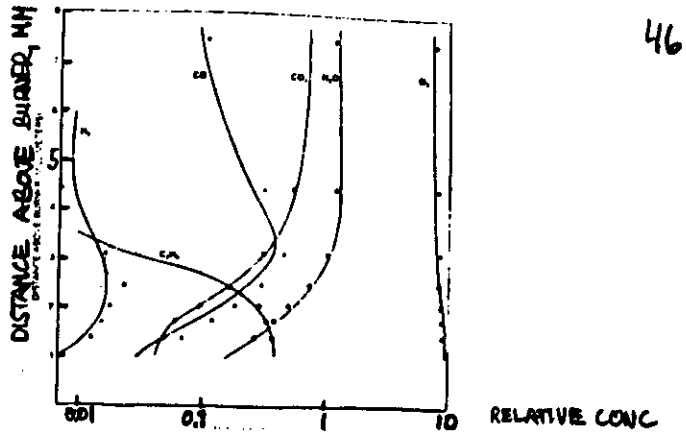

Fig. 10.1. Experimental and theoretical concentration profiles for an ethane/oxygen flame. [From 10.2].

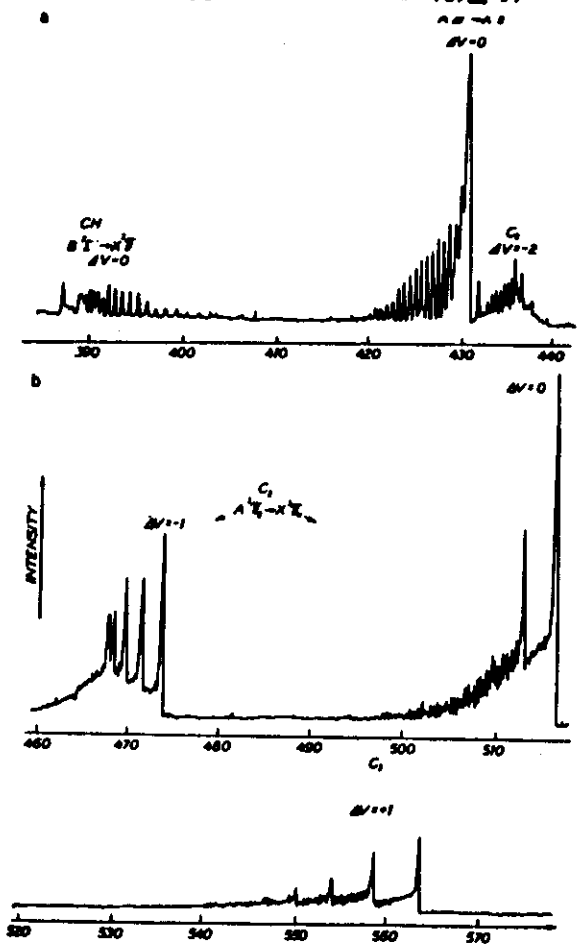

Fig. 10.2. Emission from a propane/air Bunsen burner flame. [From].

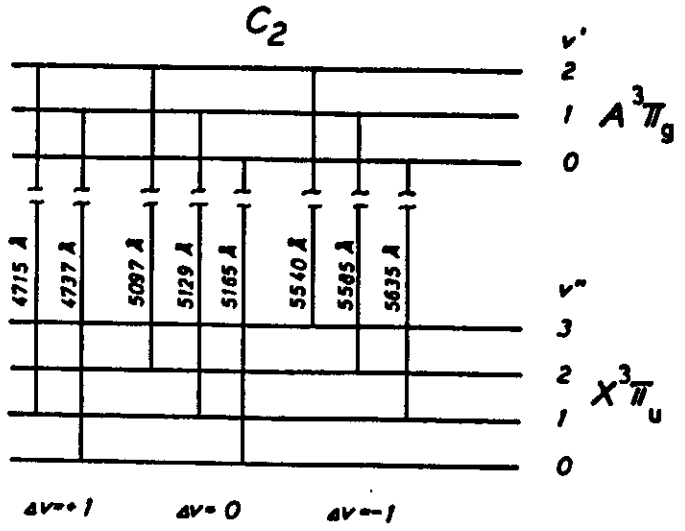

Fig. 10.3. Energy level scheme for the C_2 molecule [From]

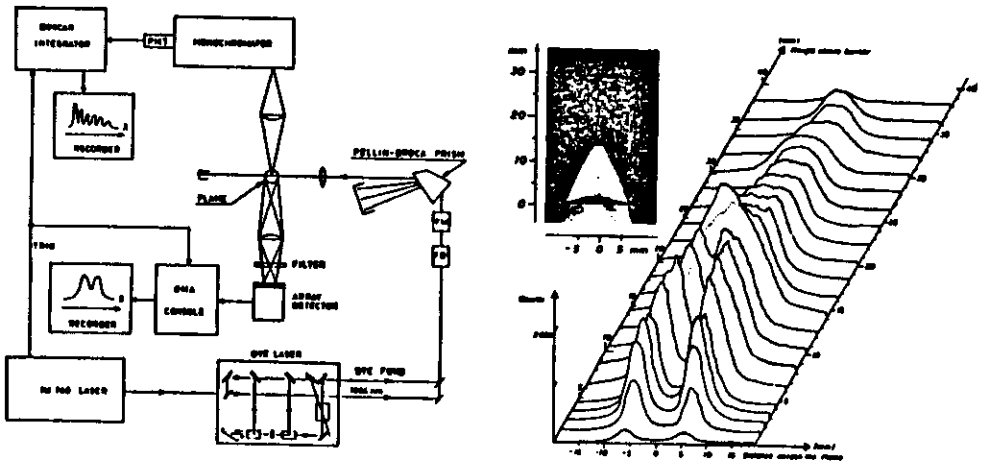

Fig. 10.4. Set-up for spectrally resolved and imaging laser-induced fluorescence studies [From 10.36].

Fig. 10.5. Spatial distributions of the OH radicals in a CH_4/O_2 flame. [From 10.10].

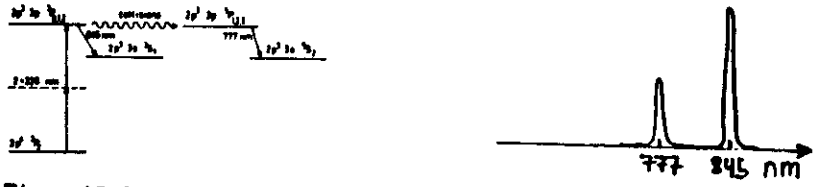

Fig. 10.6. Two-photon excitation scheme for oxygen atoms [From].

Fig. 10.7. Laser-induced fluorescence spectrum from oxygen atoms in an C_2H_2 welding torch. [From].

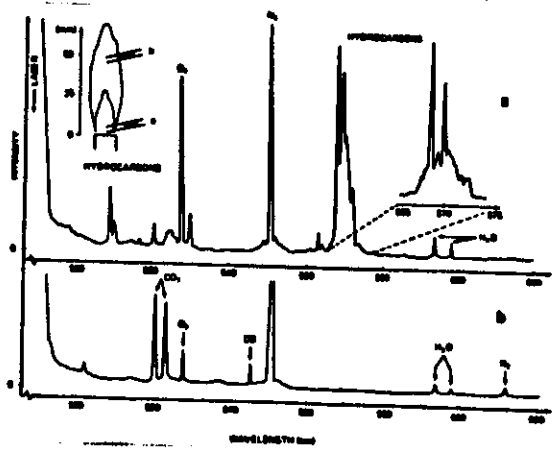

Fig. 10.8. Raman spectra of extracted flame gases at two different heights in a Bunsen burner flame. [From].

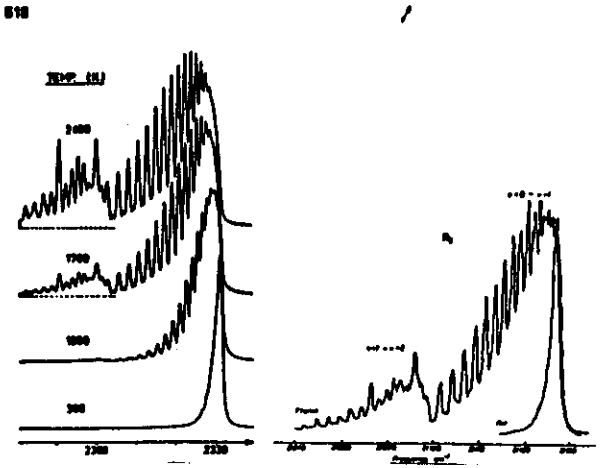

Fig. 10.9. Theoretically calculated CARS curves for N_2 molecules at different temperatures [From 10.24].

Fig. 10.10. Experimental CARS recordings for room temperature N_2 molecules and for N_2 molecules in a flame. [From 10.24].

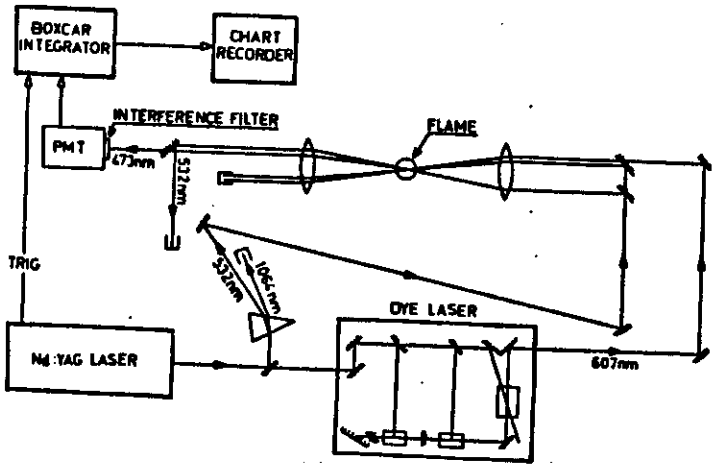

Fig. 10.11. Experimental set-up for CARS spectroscopy using the BOXCARS phasematching scheme [From].

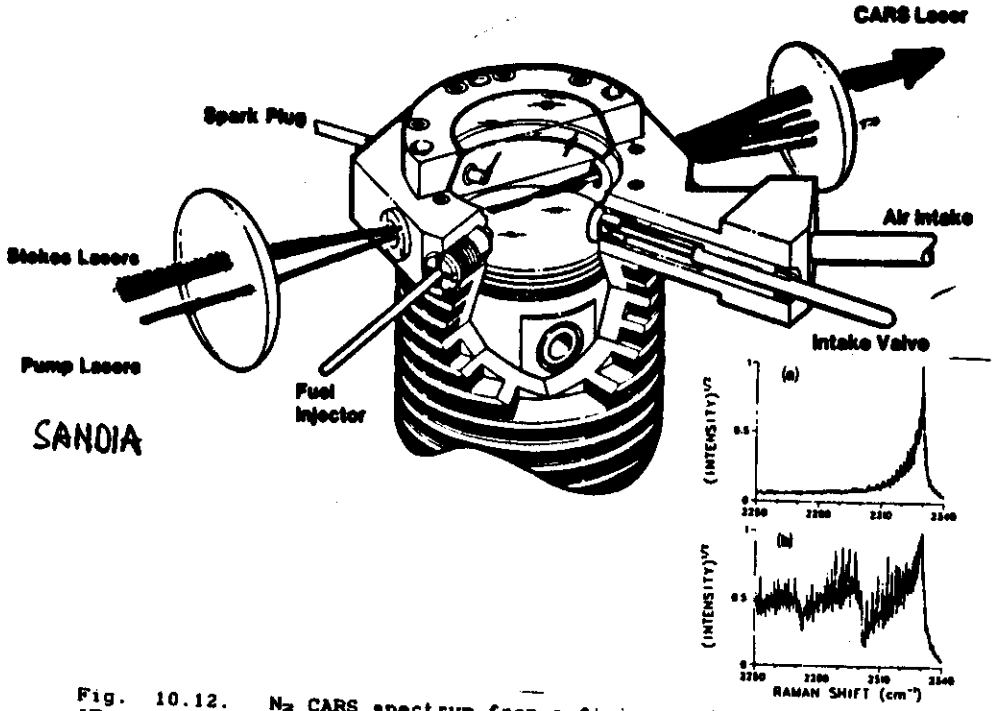

Fig. 10.12. N_2 CARS spectrum from a firing engine. [From].

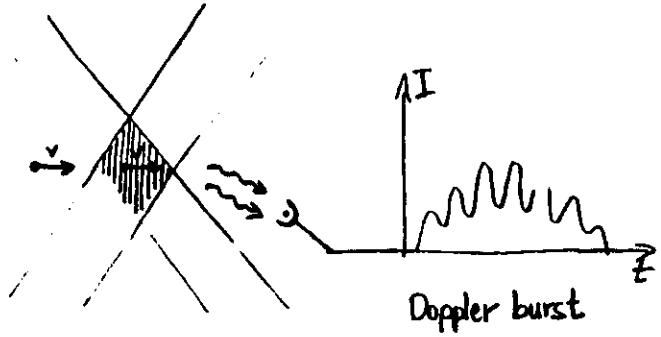

Fig. 10.13. Principle of Laser Doppler Velocimetry (LDV). [From].

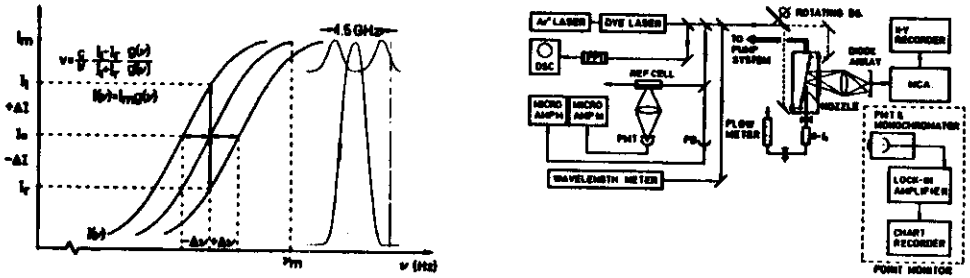

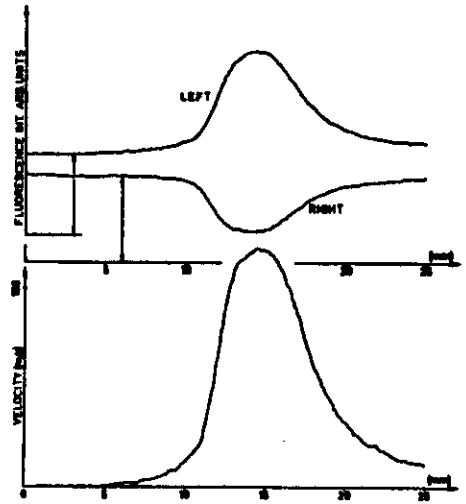

Fig. 10.14. Spectroscopic flow measurement. [From 10.35].

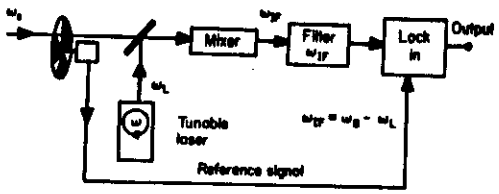

Fig. 10.15. Optical heterodyne detection. [From 10.53].

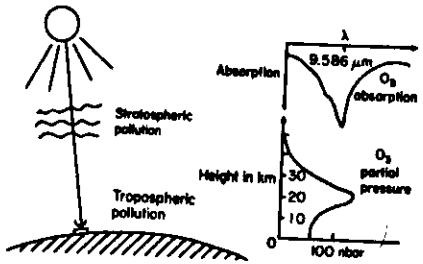

Fig. 10.16. Vertical ozon profiling. [From 10.53].

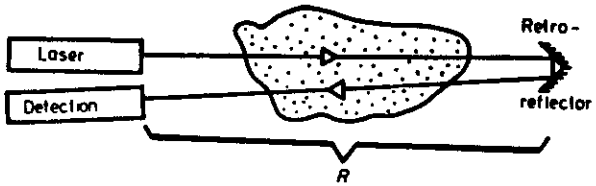

Fig. 10.17. Long path absorption measurement of atmospheric pollutants.

Fig. 10.18. Long path absorption measurement of the CO concentration across a highway. [From].

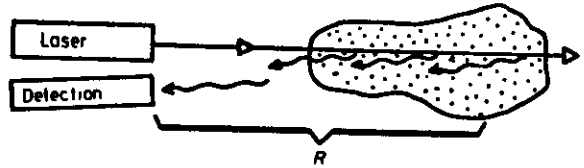

Fig. 10.19. The principle of lidar.

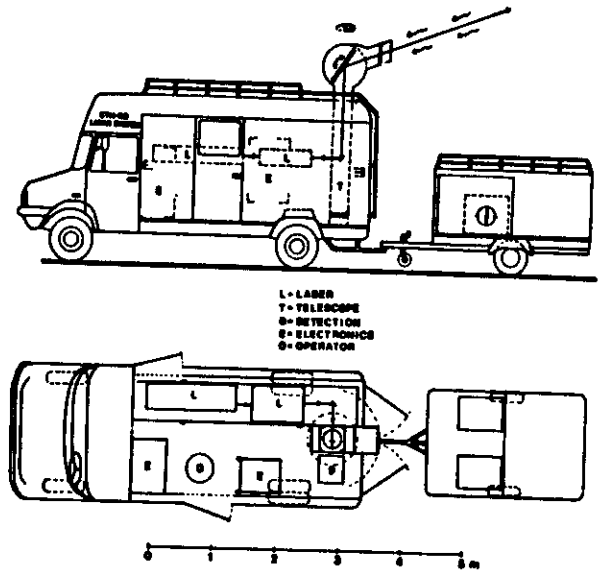

Mobilt laser-radar system.

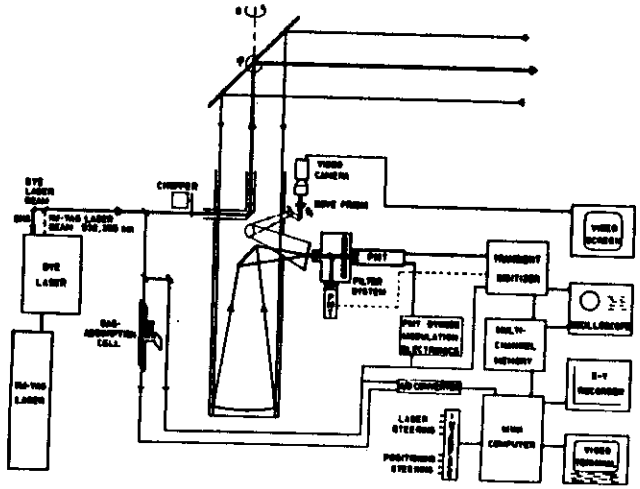

Fig. 10.20. Construction of a mobile lidar system. a) general lay out. b) optical and electronic systems. [From].

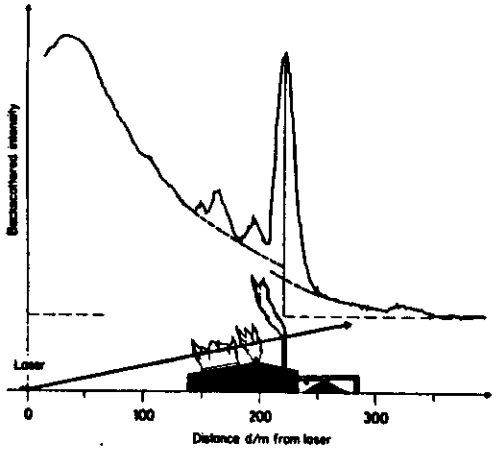

Fig. 10.21. Lidar particle monitoring [From].

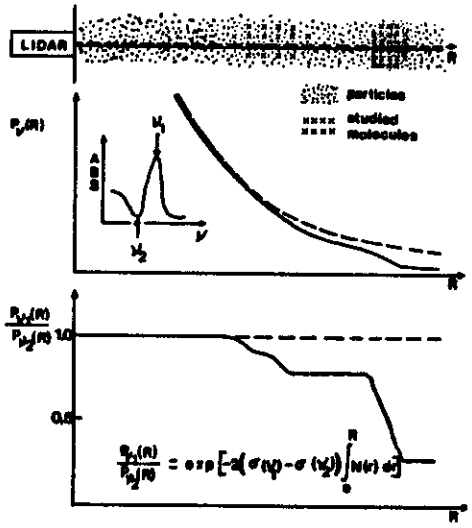

Fig. 10.22. Illustration of the dial principle. [From 10.53].

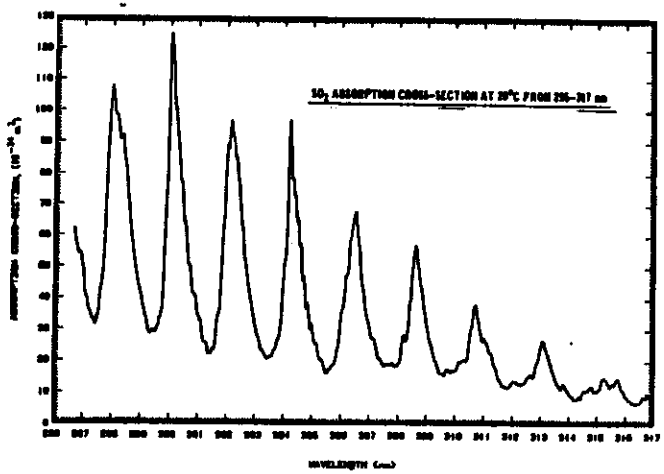

Fig. 10.23. SO_2 absorption spectrum. [From].

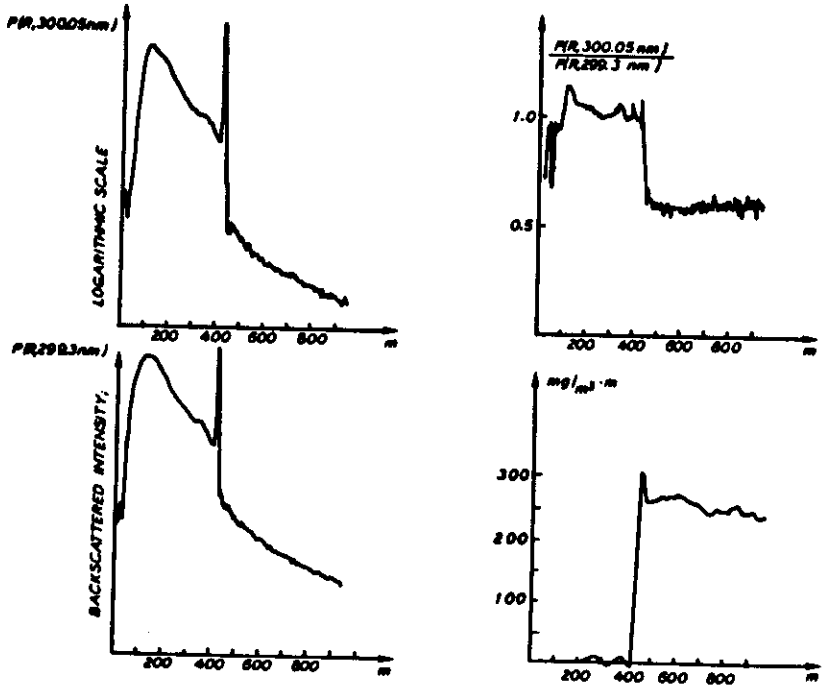

Fig. 10.24. SO_2 dial measurement. [From].

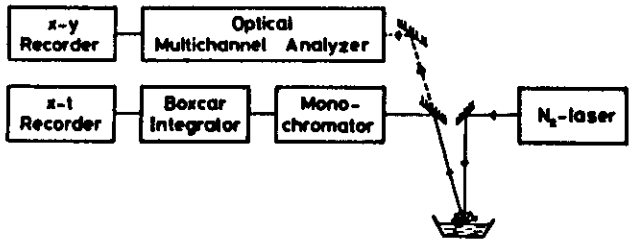

Fig. 10.25. Laboratory set-up for LIF measurements. [From].

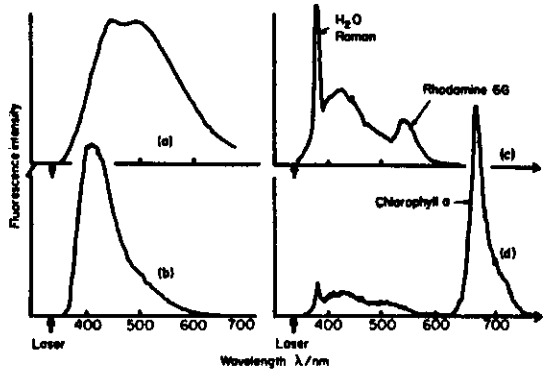

Fig. 33. Fluorescence spectra of various samples irradiated with a pulsed nitrogen laser, operating at 337 nm (intensities are not normalized) (Svanberg 1979). (a) Crude oil, Abu Dhabi. (b) River water down-stream from a sodium sulphite pulp mill. The fluorescence is about 30 times stronger than that from 'clean' water. (c) Sea water, Kattegat, containing 3 μg/l Rhodamine-6G dye. The Raman peak from water is also seen. (d) The green algae *Chlorella ovalis* Butcher in sea water.

Fig. 10.26. LIF spectra for marine substances [From 10.53].

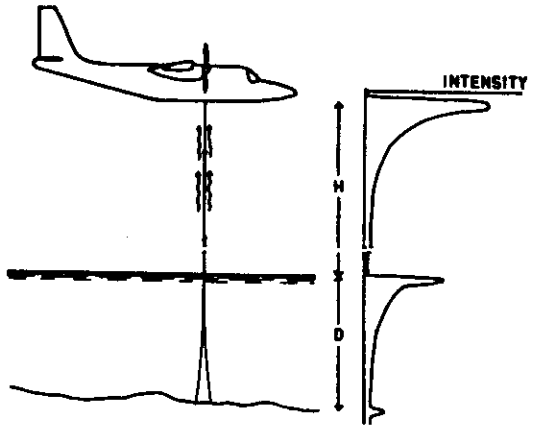

Fig. 10.27. Principle of airborne laser bathymetry [From 10.53].

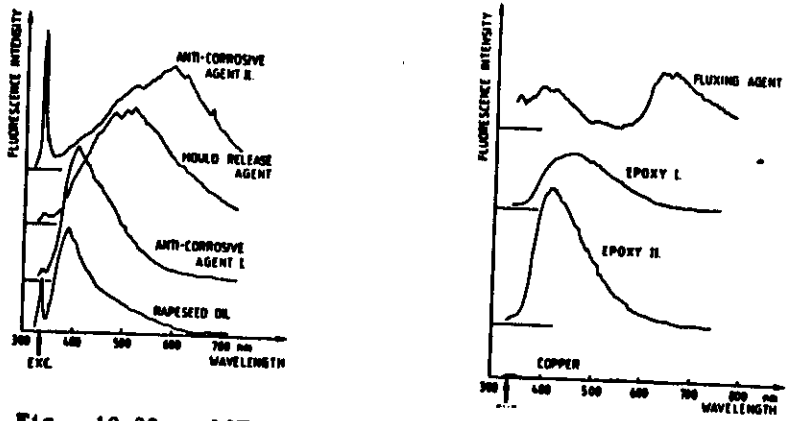

Fig. 10.28. LIF spectra of industrial surface layers. [From 10.73].

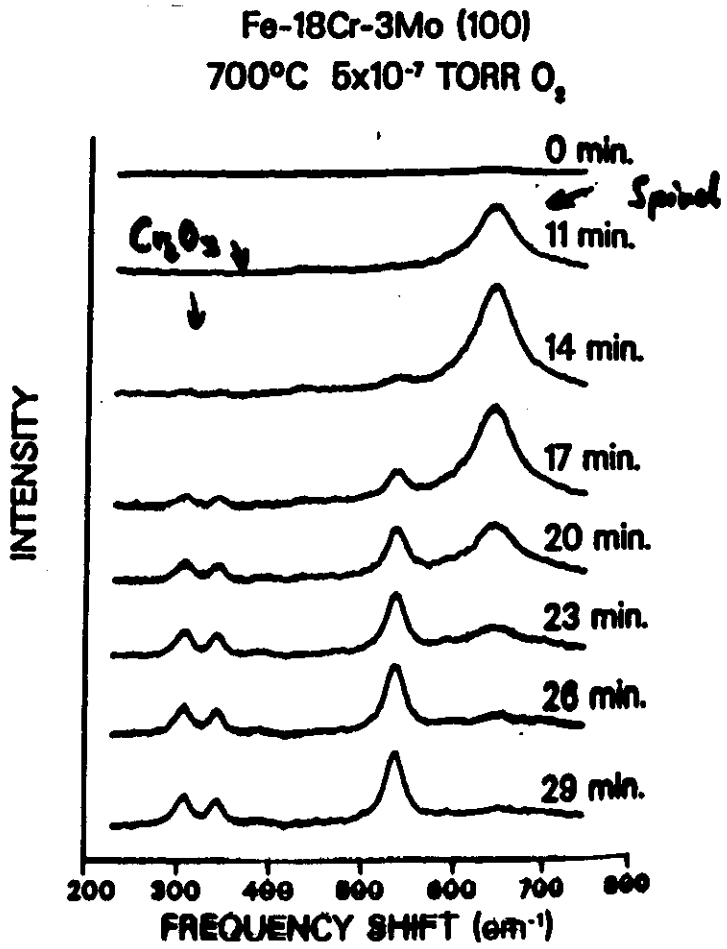

Fig. 10.30. Surface Raman spectra showing oxidation process [From].

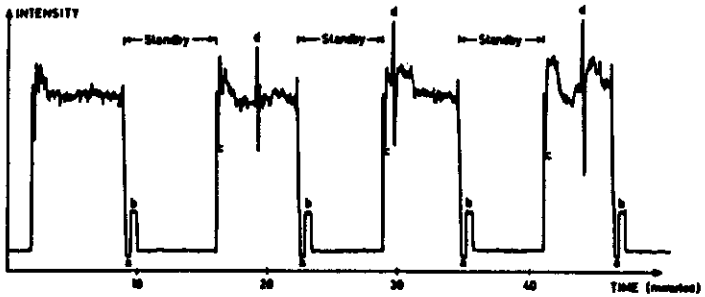

Fig. 10. Recording at the end of the continuous annealing line at SSAB, Domnarvet, Borlänge, Sweden. The coiling of four steel rolls with varying oil film thickness is monitored. At *a* the coil was removed, at *b* the strip guide was placed around the cooler and at *c* the bale wrapper passed the measuring point. At *d* the band was stopped to measure the width and thickness of the strip

Fig. 10.29. Rust oil application monitoring in a steel roll mill. [From 10.67].

Fig. 10.31. Surface monitoring by observing the generation of frequency-doubled light. [From].

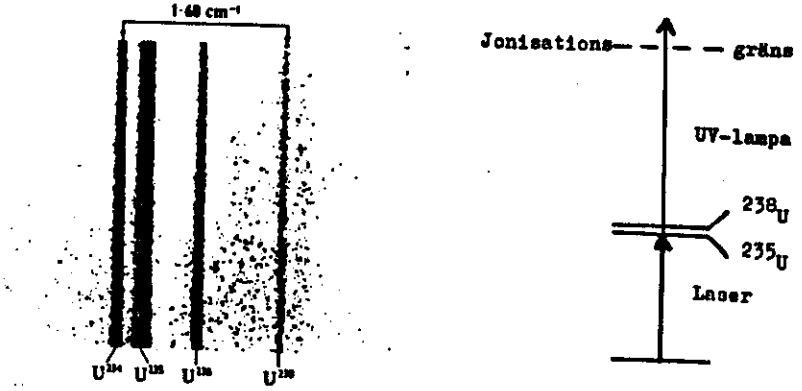

Fig. 10.32. Isotope shifts in a uranium line. [From].

Fig. 10.33. A schematic uranium isotope separation scheme.

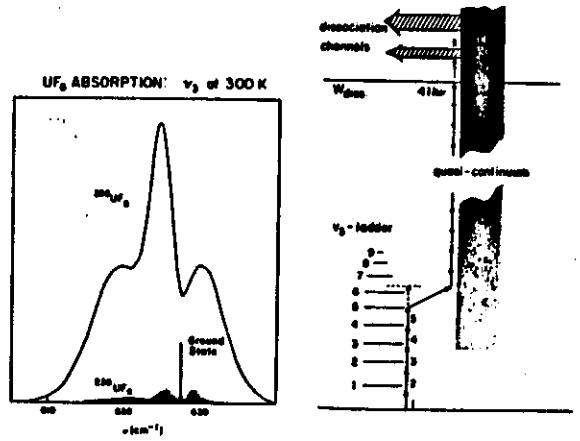

Fig. 10.34. Multi-photon dissociation process. [From].

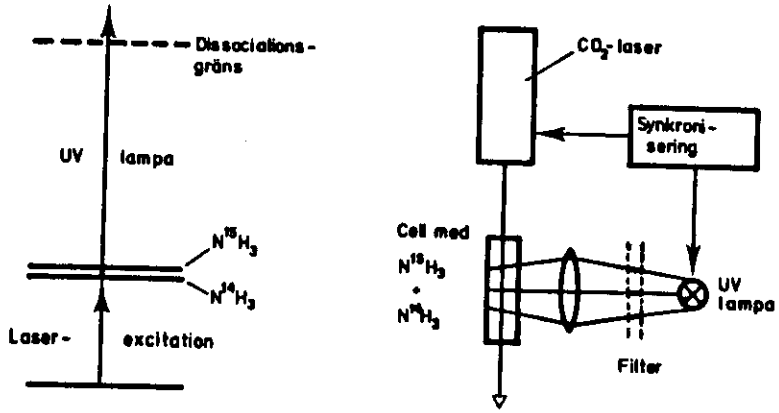

Fig. 10.35. Ammonia separation scheme. [From].

Fig. 10.36. Set-up for ammonia separation. [From].

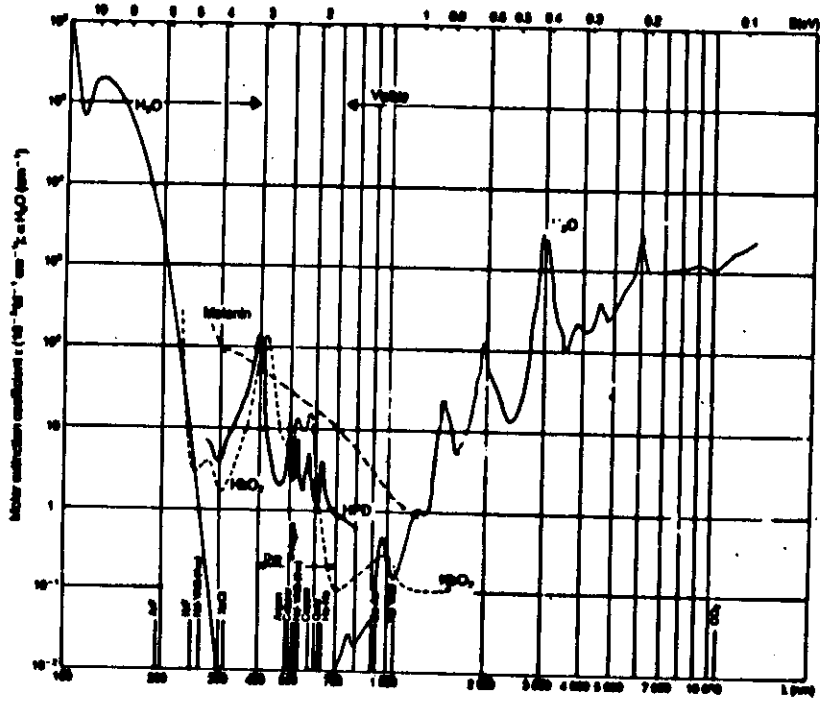

Fig. 10.37. Absorption curves for tissue constituents. [From (D.83].

Fig. 10.38. Absorption curves for different parts of the eye. [From].

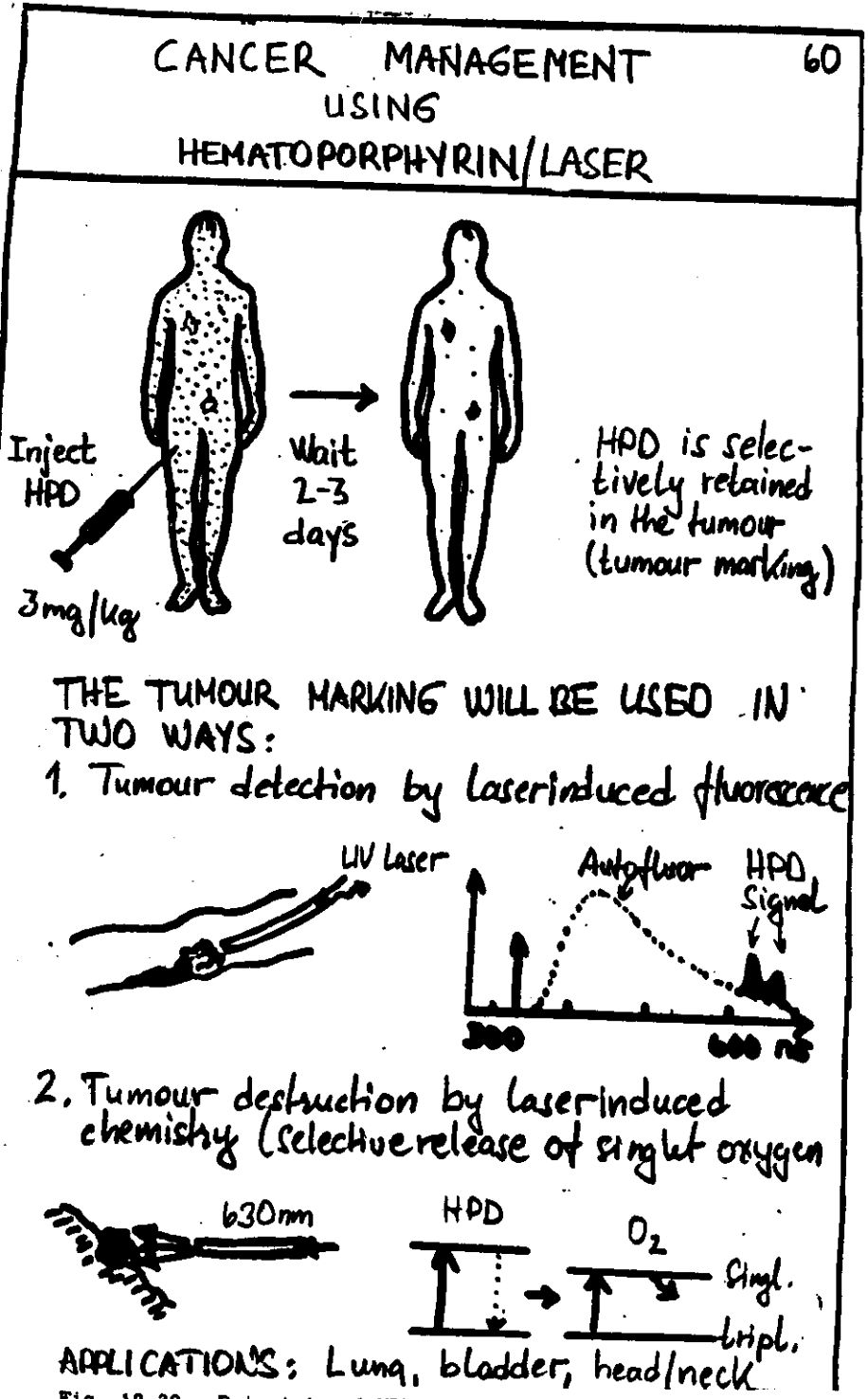

Fig. 10.39. Principle of HPD-PDT. [From].

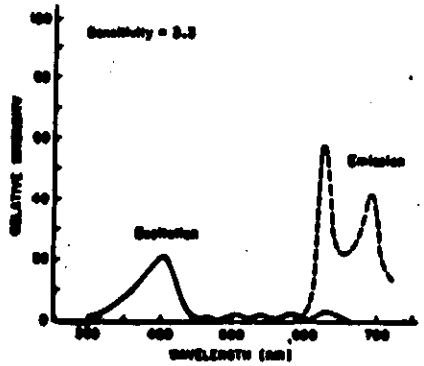

Fig. 10.40. HPD absorption and fluorescence. [From].

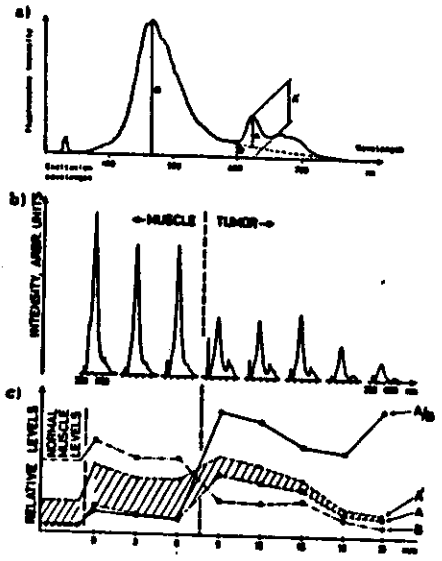

Fig. 10.41. Spectra recorded at different points across a rat tumor in muscle. Demonstration of contrast enhancement. [From].